PHYSICAL REVIEW D **81,** 024030 (2010)

Spacetime and orbits of bumpy black holes

Sarah J. Vigeland and Scott A. Hughes

Department of Physics and MIT Kavli Institute, Massachusetts Institute of Technology, 77 Massachusetts Avenue, Cambridge, Massachusetts 02139, USA

(Received 9 November 2009; published 21 January 2010)

Our Universe contains a great number of extremely compact and massive objects which are generally accepted to be black holes. Precise observations of orbital motion near candidate black holes have the potential to determine if they have the spacetime structure that general relativity demands. As a means of formulating measurements to test the black hole nature of these objects, Collins and Hughes introduced "bumpy black holes": objects that are almost, but not quite, general relativity's black holes. The spacetimes of these objects have multipoles that deviate slightly from the black hole solution, reducing to black holes when the deviation is zero. In this paper, we extend this work in two ways. First, we show how to introduce bumps which are smoother and lead to better behaved orbits than those in the original presentation. Second, we show how to make bumpy Kerr black holes—objects which reduce to the Kerr solution when the deviation goes to zero. This greatly extends the astrophysical applicability of bumpy black holes. Using Hamilton-Jacobi techniques, we show how a spacetime's bumps are imprinted on orbital frequencies, and thus can be determined by measurements which coherently track the orbital phase of a small orbiting body. We find that in the weak field, orbits of bumpy black holes are modified exactly as expected from a Newtonian analysis of a body with a prescribed multipolar structure, reproducing well-known results from the celestial mechanics literature. The impact of bumps on strong-field orbits is many times greater than would be predicted from a Newtonian analysis, suggesting that this framework will allow observations to set robust limits on the extent to which a spacetime's multipoles deviate from the black hole expectation.

DOI: 10.1103/PhysRevD.81.024030 PACS numbers: 04.25.Nx, 04.30.Db, 04.70.Bw

I. INTRODUCTION

A. Motivation: Precision tests of the black hole hypothesis

Though observations of gravitational systems agree well with the predictions of general relativity (GR), the most detailed and quantitative tests have so far been done in the weak field. ("Weak field" means that the dimensionless Newtonian potential $\phi \equiv GM/rc^2 \ll 1$, where M is a characteristic mass scale and r a characteristic distance.) This is largely because many of the most precise tests are done in our solar system (e.g., [1]). Even the celebrated tests which use binary neutron stars (e.g., [2]) are essentially weak field: for those systems, $M \sim$ several $M_\odot$, $r =$ orbital separation $\sim$ several $R_\odot$, so $\phi \sim$ a few $\times\, GM_\odot/R_\odot c^2 \sim$ a few $\times\, 10^{-6}$.

This situation is on the verge of changing. Observational technology is taking us to a regime where we either are or soon will be probing motion in strong gravity, with $\phi \gtrsim 0.1$. Examples of measurements being made now include radio studies of accretion flows near the putative black hole in our galactic center [3] and x-ray studies that allow precise measurements of accretion disk geometries [4,5]. Future measurements include the possible discovery of a black hole–pulsar system, perhaps with the Square Kilometer Array [6], and gravitational-wave observations of small bodies spiraling into massive black holes due to the backreaction of gravitational-wave emission [7].

For weak-field studies, a well-developed paradigm for testing gravity has been developed. The parametrized post-Newtonian (PPN) expansion [8,9] quantifies various measurable aspects of relativistic gravity. For example, the PPN parameter γ (whose value is 1 in GR) quantifies the amount of spatial curvature produced by a unit of rest mass. Other PPN parameters quantify a theory's nonlinearity, the degree to which it incorporates preferred frames, and the possible violation of conservation laws. See Ref. [9], Chap. 4, for a detailed discussion. Unfortunately, no similar framework exists for strong-field studies. If we hope to use observations as tools for testing the nature of strong-gravity objects and strong-field gravity, we need to rectify this.

Black holes are of particular interest for studying strong-field gravity. Aside from having the strongest accessible gravitational fields of any object in the Universe,[1] within GR they have an amazingly simple spacetime structure: the "no-hair" theorems [10–14] guarantee that the exterior

[1]More accurately, they have the largest potential $\phi \sim GM/Rc^2$. One may also categorize weak or strong gravity using spacetime curvature or tides; arguably this is a more fundamental measure for assessing whether GR is likely to be accurate or not. From this perspective, black holes are actually not such "strong-gravity" objects; indeed, the tidal field just outside a $10^8 M_\odot$ black hole's event horizon is not much different from the tidal field at the surface of the Earth. See Ref. [4] for further discussion of this point.

spacetime of any black hole is completely described by only two numbers, its mass M and spin parameter a. Any deviation from that simplicity points to a failure either in our understanding of gravity or in the nature of ultracompact objects.

Recent work by Brink [15] has reviewed in detail the challenges involved in testing the spacetime structure of massive compact bodies when one relaxes the assumption that the spacetime is Kerr. As in Brink's discussion, we will focus on spacetimes that are stationary, axisymmetric, and vacuum in some exterior region. An especially useful parametrization is provided by the work of Geroch [16] and Hansen [17]. They demonstrate that such a spacetime is completely specified by a set of mass multipole moments M_l and current multipole moments S_l. For a fluid body, M_l describes the angular distribution of the body's mass, and S_l describes the angular distribution of mass flow. In Newtonian theory, M_l labels a piece of the gravitational potential that varies as $Y_{l0}(\theta, \phi)/r^{l+1}$. There is no Newtonian analog to S_l. In the weak-field limit of GR, they label a magneticlike contribution to gravity and are reminiscent of magnetic moments.

In general, the moments $\{M_l, S_l\}$ can be arbitrary. For black holes, they take special values: a Kerr spacetime has [17]

$$M_l + iS_l = M(ia)^l \tag{1.1}$$

(in units with $G = 1 = c$; we neglect the astrophysically uninteresting possibility of the hole having macroscopic charge). In other words, only two moments out of the set $\{M_l, S_l\}$ are independent: $M_0 = M$, and $S_1 = aM$. Once those two moments have been specified, all other moments are fixed by Eq. (1.1) if the spacetime is Kerr.

Testing the hypothesis that an object is a Kerr black hole can thus be framed as a null experiment. First, measure the putative black hole spacetime's multipoles. Using the moments M_0 and S_1, determine the parameters M and a. If the spacetime is Kerr, all moments for $l \geq 2$ must be given by Eq. (1.1). The null hypothesis is that any deviation from those Kerr moments is zero. Failure of the null hypothesis means the black hole candidate is not a Kerr black hole, and may indicate a failure of strong-field GR.

B. Bumpy black holes: Past work

Performing this null experiment requires strong-field spacetimes with multipoles differing from those of black holes. Given the tremendous success of general relativity and the black hole hypothesis at explaining a wide span of data, a reasonable starting point is to consider spacetimes whose multipoles deviate only slightly. Imagine starting with a spacetime whose Geroch-Hansen moments satisfy

$$M_l + iS_l = M(ia)^l + \delta M_l + i\delta S_l. \tag{1.2}$$

The null hypothesis—black hole candidates are described by GR's Kerr metric—means $\delta M_l = 0$, $\delta S_l = 0$ for all l.

To this end, Collins and Hughes [18] (hereafter CH04) introduced the bumpy black hole: a spacetime that deviates in a small, controllable manner from the exact black holes of GR. By construction, the bumpy black hole includes "normal" black holes as a limit. This is central to testing the black hole hypothesis by a null experiment. Spacetimes of other proposed massive, compact objects (for example, boson stars [19,20]) typically do not include black holes as a limiting case. This limits their utility if black hole candidates are, in fact, GR's black holes. Measurements of black holes using observables formulated in a bumpy black hole spacetime should simply measure the spacetime's "bumpiness" (defined more precisely below) to be zero.

Though a useful starting point, the bumpy black holes developed in CH04 had two major shortcomings. First, the changes to the spacetime that were introduced to modify its multipole moments were not smooth. The worked example presented in CH04 is interpreted as a Schwarzschild black hole perturbed by an infinitesimally thin ring of positive mass around its equator and by a pair of negative mass infinitesimal points near its poles. Though this changes the spacetime's quadrupole moment (the desired outcome of this construction), it gives the spacetime a pathological strong-field structure. This is reflected in the fact that nonequatorial strong-field orbits are ill behaved in the CH04 construction [21].

Second, CH04 only examined bumpy Schwarzschild black holes. Although their approach differed in many details from that used in CH04, Glampedakis and Babak [22] (hereafter GB06) rectified this deficiency with their introduction of a "quasi-Kerr" spacetime. Their construction uses the exterior Hartle-Thorne metric [23,24] describing the exterior of any slowly rotating, axisymmetric, stationary body. It includes the Kerr metric to $\mathcal{O}(a^2)$ as a special case. Identifying the influence of the quadrupole moment in the Hartle-Thorne form of the Kerr metric, they then introduce a modification to the full Kerr spacetime that changes the black hole's quadrupole moment from its canonical value.

C. This analysis

The goal of this work is to rectify the deficiencies of CH04 and to extend the bumpy black hole concept to spinning black holes. Dealing with the nonsmooth nature of the bumps presented in CH04 is, as we show in Secs. II, IV, and V, quite straightforward. It simply requires introducing perturbations to the black hole background that are smooth rather than discontinuous. In essence, rather than having bumps that correspond to infinitesimal points and rings, the bumps we use here are smeared into pure multipoles.

Extending CH04 to spinning black holes is more of a challenge. Given that GB06 already introduced a bumpy-black-hole-like spacetime that encompasses spacetimes with angular momentum, one might wonder why another

construction is needed. A key motivation is that we would like to be able to make an arbitrary modification to a black hole's moments. Although showing that a black hole candidate has a non-Kerr value for the quadrupole moment would be sufficient to falsify its black hole nature (at least within the framework of GR), one can imagine scenarios in which the first L moments of a black hole candidate agree with the Kerr value, but things differ for $l > L$. For example, Yunes and Pretorius have shown that in Chern-Simons modifications to GR, slowly rotating black hole solutions have the multipolar structure of Kerr for $l < 4$, but differ for $l \geq 4$ [25]. There are many ways in which black hole candidates might differ from the black holes of general relativity; we need to develop a toolkit sufficiently robust that it can encompass these many potential points of departure.

Our technique for making bumpy Kerr holes is based on the Newman-Janis algorithm [26]. This algorithm transforms a Schwarzschild spacetime into Kerr by "rotating" the spacetime in a complex configuration space.[2] In this paper, we construct bumpy Kerr black holes by applying the Newman-Janis algorithm to bumpy Schwarzschild black holes. The outcome of this procedure is a spacetime whose mass moments are deformed relative to Kerr. When the bumpiness is set equal to zero, we recover the Kerr metric. A companion paper [28] examines the multipolar structure of bumpy Kerr black holes in more detail, demonstrating that one can construct a spacetime in which the mass moments deviate arbitrarily from Kerr (provided that they are small).

Once one has constructed a bumpy black hole spacetime, one then needs to show how its bumps are encoded in observables. The most detailed quantitative tests will come from orbits near black hole candidates. As such, it is critical to know how orbital frequencies change as a function of a spacetime's bumpiness. More generally, we are faced with the problem of understanding motion in general stationary axisymmetric vacuum spacetimes. Brink [29] has recently published a very detailed analysis of this problem, with a focus on understanding whether and for which situations the spacetimes admit integrable motion. She has found evidence that geodesic motion in such spacetimes may, in many cases, be integrable. If so, the problem of mapping general spacetimes (not just "nearly black hole" spacetimes) may be tractable. Gair, Li, and Mandel [30] have similarly examined orbital characteristics in the Manko-Novikov spacetime [31], which has a particular tunable non-Kerr structure. They show how orbits change in such spacetimes, and how their bumpiness colors observable characteristics.

[2]This complex "rotation" is made most clear by framing the discussion using the Ernst potential [27]. Transforming from Schwarzschild to Kerr corresponds to adding an imaginary part to a particular potential. Further discussion is given in a companion paper [28].

For this analysis, we confine ourselves to the simpler problem of motion in bumpy black hole spacetimes, addressing this challenge in Secs. IV and V using canonical perturbation theory. As is now well known (and was shown rather spectacularly by Schmidt [32]), Hamilton-Jacobi methods let us write down closed-form expressions for the three orbital frequencies $(\Omega^r, \Omega^\theta, \Omega^\phi)$ which completely characterize the behavior of bound Kerr black hole orbits. Since bumpy black hole spacetimes differ only perturbatively from black hole spacetimes, canonical perturbation theory lets us characterize how a spacetime's bumps shift those frequencies, and thus are encoded in observables. Similar techniques were used in GB06 to see how frequencies are shifted in a quasi-Kerr metric, and were also used by Hinderer and Flanagan [33] in a two-time-scale analysis of inspiral into Kerr black holes.

D. Organization and overview

We begin in Sec. II with an overview of the spacetimes that we study. We start with the axially symmetric and stationary Weyl line element. We first review the Einstein field equations in this representation, introduce the Schwarzschild limit, and then describe first-order perturbations. The spacetime's bumpiness is set by choosing a function ψ_1 which controls how the spacetime deviates from the black hole limit. We initially leave ψ_1 arbitrary, except for the requirement that it be small enough that terms of order $(\psi_1)^2$ can be neglected. Later in the paper, we will take ψ_1 to be a pure multipole in the Weyl representation. Following our discussion of bumpy Schwarzschild spacetimes, we show how to use the Newman-Janis algorithm to build bumpy Kerr black holes.

We study geodesic motion in these spacetimes in Sec. III. We begin by reviewing the most important properties of normal black hole orbits, reviewing Kerr geodesics in Sec. III A, and then describing how to compute orbital frequencies using Hamilton-Jacobi methods in Sec. III B. The discussion of frequencies is largely a synopsis of Schmidt's pioneering study, Ref. [32]. We then show how these techniques can be adapted, using canonical perturbation theory, to bumpy black holes (Sec. III C). Canonical perturbation theory requires averaging a bump's shift to an orbit's Hamiltonian. This averaging was developed in Ref. [34], and is summarized in Appendix A.

We present our results for bumpy Schwarzschild and bumpy Kerr orbits in Secs. IV and V, respectively. We take ψ_1 to be a pure multipole in the Weyl sector, construct the spacetime, and numerically compute the shifts in Ω^r, Ω^θ, and Ω^ϕ. Detailed results are given for $l = 2$, $l = 3$, and $l = 4$. There is no reason in principle to stop there, though the results quickly become repetitive. Section IV gives our results for bumpy Schwarzschild black holes, and Sec. V gives results for bumpy Kerr.

A few results are worth highlighting. First, we find that the exact numerical results for frequency shifts correctly

reproduce the Newtonian limit as our orbits are taken into the weak field. (We develop this limit in some detail in Appendix B to facilitate the comparison.) The frequency shifts are substantially enhanced in the strong field. The shift to the radial frequency is particularly interesting: it tends to oscillate, shifting between an enhancement and a decrement as orbits move into the strong field. This behavior appears to be a robust signature of non-Kerr multipole structure in black hole strong fields.

Interestingly, it turns out that black hole spin does not have a very strong impact on the bumpiness-induced shifts to orbital frequencies. Spin's main effect is to change the location of the last stable orbit. For large spin, orbits reach deeper into the strong field, amplifying the bumps' impact on orbital frequencies. Aside from the change to the last stable orbits, the impact of a particular multipolar bump looks largely the same across all spin values. Some examples of the frequency shifts we find are shown in Figs. 1 ($l = 2$, Schwarzschild), 2 ($l = 4$, Schwarzschild), and 3 ($l = 2$, Kerr). (We have no figures for $l = 3$ since the secular shifts to orbital frequencies are zero in that case, as they are for all odd values of l. We also do not show results for $l = 4$ bumps of Kerr black holes since, as discussed above, they are very similar to the $l = 4$ Schwarzschild results.)

Finally, we summarize our analysis and suggest some directions for future work in Sec. VI. Among the points we note are that, in this analysis, we only consider changes to the mass moments of the black hole spacetime. Adding ''current-type'' bumps to a spacetime is discussed in a companion paper [28]. We also do not discuss in this analysis the issue of measurability. Turning these foundations for mapping the multipole moment structure of black holes into a practical measurement program (for instance, via gravitational-wave measurements, timing of a black hole–pulsar binary, or precision mapping in radio or x rays of accretion flows) will take a substantial effort.

Throughout this paper, we work in geometrized units with $G = c = 1$; a useful conversion factor in these units is $1M_\odot = 4.92 \times 10^{-6}$ seconds. When we discuss bumpy black holes, we will always use a ''hat'' accent to denote quantities which are calculated in the pure black hole background spacetimes. For example, an orbital frequency is written $\Omega = \hat{\Omega} + \delta\Omega$; $\hat{\Omega}$ is the frequency of an orbit in the black hole background, and $\delta\Omega$ denotes the shift due to the black hole's bumps.

II. BLACK HOLE AND BUMPY BLACK HOLE SPACETIMES

We begin with general considerations on the spacetimes we consider. Since we focus on stationary, axisymmetric spacetimes, the Weyl metric [35] is a good starting point:

$$ds^2 = -e^{2\psi}dt^2 + e^{2\gamma-2\psi}(d\rho^2 + dz^2) + e^{-2\psi}\rho^2 d\phi^2. \tag{2.1}$$

The nontrivial vacuum Einstein equations for this metric are given by

$$0 = \frac{\partial^2\psi}{\partial\rho^2} + \frac{1}{\rho}\frac{\partial\psi}{\partial\rho} + \frac{\partial^2\psi}{\partial z^2}, \tag{2.2}$$

$$\frac{\partial\gamma}{\partial\rho} = \rho\left[\left(\frac{\partial\psi}{\partial\rho}\right)^2 - \left(\frac{\partial\psi}{\partial z}\right)^2\right], \tag{2.3}$$

$$\frac{\partial\gamma}{\partial z} = 2\rho\frac{\partial\psi}{\partial\rho}\frac{\partial\psi}{\partial z}. \tag{2.4}$$

Equations (2.2), (2.3), and (2.4) will be our main tools for building bumpy black hole spacetimes. We will put $\psi = \psi_0 + \psi_1$, $\gamma = \gamma_0 + \gamma_1$, with $\psi_1/\psi_0 \ll 1$, and $\gamma_1/\gamma_0 \ll 1$. Before specializing to black hole backgrounds, note that Eq. (2.2) is simply Laplace's equation. The functions ψ_1 can thus very conveniently be taken to be harmonic functions. This is key to smoothing out the spacetime's bumps and curing one of the deficiencies of CH04.

A. Schwarzschild and bumpy Schwarzschild

We begin by building a bumpy Schwarzschild black hole. The Schwarzschild metric is recovered from Eq. (2.1) when $\psi_1 = \gamma_1 = 0$ and we set

$$\psi_0 = \ln\tanh(u/2), \tag{2.5}$$

$$\gamma_0 = -\frac{1}{2}\ln\left(1 + \frac{\sin^2 v}{\sinh^2 u}\right). \tag{2.6}$$

The prolate spheroidal coordinates (u, v) are a remapping of the coordinates (ρ, z) used in Eq. (2.1):

$$\rho = M\sinh u\sin v, \tag{2.7}$$

$$z = M\cosh u\cos v. \tag{2.8}$$

(Below we will remap these to the familiar Schwarzschild form.) Expanding the Einstein equations Eqs. (2.2), (2.3), and (2.4) about these Schwarzschild values to leading order in ψ_1 and γ_1, the perturbations must satisfy

$$\nabla^2\psi_1 = 0, \tag{2.9}$$

$$\frac{\partial\gamma_1}{\partial u} = \frac{2[\tan v(\partial\psi_1/\partial u) + \tanh u(\partial\psi_1/\partial v)]}{\sinh u(\coth u\tan v + \tanh u\cot v)}, \tag{2.10}$$

$$\frac{\partial\gamma_1}{\partial v} = \frac{2[\tan v(\partial\psi_1/\partial v) - \tanh u(\partial\psi_1/\partial u)]}{\sinh u(\coth u\tan v + \tanh u\cot v)}. \tag{2.11}$$

As discussed in CH04, Eqs. (2.10) and (2.11) actually overdetermine the solution; we will use Eq. (2.11) to calculate γ_1. [Note also that the $\tan v$ in the numerator of Eq. (2.10) is incorrectly written $\cot v$ in CH04.]

To connect this to the variables we will use later in the paper (and to put it in a more familiar form), we make a final change of coordinates, putting

$$r = 2M\cosh^2(u/2), \tag{2.12}$$

$$\theta = v, \tag{2.13}$$

so that

$$\rho = r\sin\theta\sqrt{1-\frac{2M}{r}}, \tag{2.14}$$

$$z = (r-M)\cos\theta. \tag{2.15}$$

The spacetime then becomes

$$\begin{aligned} ds^2 &= -e^{2\psi_1}\left(1-\frac{2M}{r}\right)dt^2 + e^{2\gamma_1-2\psi_1}\left(1-\frac{2M}{r}\right)^{-1}dr^2 \\ &\quad + r^2e^{2\gamma_1-2\psi_1}d\theta^2 + r^2\sin^2\theta e^{-2\psi_1}d\phi^2 \\ &\equiv (\hat{g}_{\alpha\beta} + b_{\alpha\beta})dx^\alpha dx^\beta. \end{aligned} \tag{2.16}$$

Although we have left the potentials ψ_1 and γ_1 in exponential form, these quantities must be expanded to first order, since we solve for them using linearized Einstein equations. We use the exponential form only for notational convenience. On the second line, $\hat{g}_{\alpha\beta}$ is the Schwarzschild metric, and

$$b_{tt} = -2\psi_1\left(1-\frac{2M}{r}\right), \tag{2.17}$$

$$b_{rr} = (2\gamma_1 - 2\psi_1)\left(1-\frac{2M}{r}\right)^{-1}, \tag{2.18}$$

$$b_{\theta\theta} = (2\gamma_1 - 2\psi_1)r^2, \tag{2.19}$$

$$b_{\phi\phi} = -2\psi_1 r^2\sin^2\theta. \tag{2.20}$$

All other components of $b_{\alpha\beta}$ are zero. We clearly recover the normal Schwarzschild black hole when $\psi_1 \to 0$, $\gamma_1 \to 0$.

B. Kerr and bumpy Kerr

We now use the Newman-Janis algorithm [26] to transform bumpy Schwarzschild into bumpy Kerr. We begin with the bumpy Schwarzschild metric written in prolate spheroidal coordinates:

$$\begin{aligned} ds^2 &= -e^{2\psi_1}\tanh^2(u/2)dt^2 + e^{2\gamma_1-2\psi_1}4M^2\cosh^4(u/2) \\ &\quad \times(du^2+dv^2) + e^{-2\psi_1}4M^2\cosh^4(u/2)\sin^2 v d\phi^2. \end{aligned} \tag{2.21}$$

The first step in the Newman-Janis algorithm uses the fact that the metric can be written in terms of a complex null tetrad with legs l^μ, n^ν, m^ν:

$$g^{\mu\nu} = -l^\mu n^\nu - l^\nu n^\mu + m^\mu\bar{m}^\nu + m^\nu\bar{m}^\mu; \tag{2.22}$$

an overbar denotes complex conjugate. The legs are given by

$$l^\mu = e^{-\psi_1}\coth^2(u/2)\delta^\mu_t + \frac{1}{M}e^{\psi_1-\gamma_1}\mathrm{csch}u\,\delta^\mu_u, \tag{2.23}$$

$$n^\mu = \frac{1}{2}e^{-\psi_1}\delta^\mu_t - \frac{1}{2M}e^{\psi_1-\gamma_1}\mathrm{csch}u\tanh^2(u/2)\delta^\mu_u, \tag{2.24}$$

$$m^\mu = \frac{1}{2\sqrt{2}M}e^{\psi_1}\mathrm{sech}^2(u/2)(e^{-\gamma_1}\delta^\mu_v + i\csc v\,\delta^\mu_\phi). \tag{2.25}$$

We use the Kronecker delta δ^μ_ν to indicate components. Next follows the key step of the Newman-Janis algorithm: We allow the coordinate u to be complex, and rewrite l^μ, n^μ, and m^μ as

$$\begin{aligned} l^\mu &= e^{-\psi_1}\frac{2\delta^\mu_t}{\tanh^2(u/2)+\tanh^2(\bar{u}/2)} \\ &\quad + e^{\psi_1-\gamma_1}\frac{\delta^\mu_u}{M\sqrt{\cosh u\cosh\bar{u}-1}}, \end{aligned} \tag{2.26}$$

$$n^\mu = \frac{1}{2}e^{-\psi_1}\delta^\mu_t - e^{\psi_1-\gamma_1}\frac{[\tanh^2(u/2)+\tanh^2(\bar{u}/2)]}{4M\sqrt{\cosh u\cosh\bar{u}-1}}\delta^\mu_u, \tag{2.27}$$

$$m^\mu = \frac{1}{2\sqrt{2}M}e^{\psi_1}\mathrm{sech}^2(\bar{u}/2)(e^{-\gamma_1}\delta^\mu_v + i\csc v\,\delta^\mu_\phi). \tag{2.28}$$

Notice that we recover the original tetrad when we force $u = \bar{u}$. Further discussion of this seemingly *ad hoc* procedure (and an explanation of how it uniquely generates the Kerr spacetime) is given in Ref. [36].

Next, change coordinates: Rewrite the tetrad using (U, r, θ, ϕ), given by

$$U = t - 2M\cosh^2(u/2) - 2M\ln[\sinh^2(u/2)] - ia\cos\theta, \tag{2.29}$$

$$r = 2M\cosh^2(u/2) + ia\cos\theta, \tag{2.30}$$

$$\theta = v. \tag{2.31}$$

The axial coordinate ϕ is the same in both coordinate systems. At this point, a is just a parameter. The result of this transformation is

$$l^\mu = (e^{-\psi_1} - e^{\psi_1-\gamma_1})\left(1-\frac{2Mr}{\Sigma}\right)^{-1}\delta^\mu_U + e^{\psi_1-\gamma_1}\delta^\mu_r, \tag{2.32}$$

$$n^\mu = \frac{1}{2}(e^{-\psi_1} + e^{\psi_1-\gamma_1})\delta^\mu_U - \frac{1}{2}e^{\psi_1-\gamma_1}\left(1-\frac{2Mr}{\Sigma}\right)\delta^\mu_r, \tag{2.33}$$

$$m^\mu = \frac{e^{\psi_1-\gamma_1}}{\sqrt{2}(r+ia\cos\theta)}[ia\sin\theta(\delta^\mu_U - \delta^\mu_r) + \delta^\mu_\theta + e^{\gamma_1} i\csc\theta\delta^\mu_\phi], \quad (2.34)$$

where $\Sigma = r^2 + a^2\cos^2\theta$. Making one further coordinate transformation,

$$dU = dt - \frac{r^2+a^2}{\Delta}dr, \qquad d\phi = d\phi' - \frac{a}{\Delta}dr, \quad (2.35)$$

gives us a bumpy Kerr black hole metric in Boyer-Lindquist coordinates:

$$\begin{aligned} ds^2 = &-e^{2\psi_1}\left(1-\frac{2Mr}{\Sigma}\right)dt^2 + e^{2\psi_1-\gamma_1}(1-e^{\gamma_1})\frac{4a^2Mr\sin^2\theta}{\Delta\Sigma}dtdr - e^{2\psi_1-\gamma_1}\frac{4aMr\sin^2\theta}{\Sigma}dtd\phi + e^{2\gamma_1-2\psi_1}\left(1-\frac{2Mr}{\Sigma}\right)^{-1} \\ &\times\left[1+e^{-2\gamma_1}(1-2e^{\gamma_1})\frac{a^2\sin^2\theta}{\Delta} - e^{4\psi_1-4\gamma_1}(1-e^{\gamma_1})^2\frac{4a^4M^2r^2\sin^4\theta}{\Delta^2\Sigma^2}\right]dr^2 \\ &- 2(1-e^{\gamma_1})a\sin^2\theta\left[e^{-2\psi_1}\left(1-\frac{2Mr}{\Sigma}\right)^{-1} - e^{2\psi_1-2\gamma_1}\frac{4a^2M^2r^2\sin^2\theta}{\Delta\Sigma(\Sigma-2Mr)}\right]drd\phi + e^{2\gamma_1-2\psi_1}\Sigma d\theta^2 \\ &+ \Delta\left[e^{-2\psi_1}\left(1-\frac{2Mr}{\Sigma}\right)^{-1} - e^{2\psi_1-2\gamma_1}\frac{4a^2M^2r^2\sin^2\theta}{\Delta\Sigma(\Sigma-2Mr)}\right]\sin^2\theta d\phi^2, \end{aligned} \quad (2.36)$$

where $\Delta \equiv r^2 - 2Mr + a^2$, and we have dropped the prime on ϕ. Notice that Eq. (2.36) reduces to the normal Kerr black hole metric when $\psi_1 \to 0$, $\gamma_1 \to 0$; the parameter a is seen to be the specific spin angular momentum, $|\vec{S}|/M$. A companion paper [28] examines the multipoles of this spacetime for particular choices of ψ_1 and demonstrates that it corresponds to Kerr with some moments set to the "wrong" values. The Newman-Janis algorithm applied to the bumpy Schwarzschild black hole produces a bumpy Kerr black hole.

Writing the bumpy Kerr metric in the form $g_{\alpha\beta} = \hat{g}_{\alpha\beta} + b_{\alpha\beta}$, we read out of Eq. (2.36)

$$b_{tt} = -2\left(1-\frac{2Mr}{\Sigma}\right)\psi_1, \quad (2.37)$$

$$b_{tr} = -\gamma_1\frac{2a^2Mr\sin^2\theta}{\Delta\Sigma}, \quad (2.38)$$

$$b_{t\phi} = (\gamma_1 - 2\psi_1)\frac{2aMr\sin^2\theta}{\Sigma}, \quad (2.39)$$

$$b_{rr} = 2(\gamma_1-\psi_1)\frac{\Sigma}{\Delta}, \quad (2.40)$$

$$b_{r\phi} = \gamma_1\left[\left(1-\frac{2Mr}{\Sigma}\right)^{-1} - \frac{4a^2M^2r^2\sin^2\theta}{\Delta\Sigma(\Sigma-2Mr)}\right]a\sin^2\theta, \quad (2.41)$$

$$b_{\theta\theta} = 2(\gamma_1-\psi_1)\Sigma, \quad (2.42)$$

$$b_{\phi\phi} = \left[(\gamma_1-\psi_1)\frac{8a^2M^2r^2\sin^2\theta}{\Delta\Sigma(\Sigma-2Mr)} - 2\psi_1\left(1-\frac{2Mr}{\Sigma}\right)^{-1}\right] \times \Delta\sin^2\theta. \quad (2.43)$$

Other components are related by symmetry or zero. By inspection, we can see that $b_{\alpha\beta} \to 0$ as $\psi_1 \to 0$, $\gamma_1 \to 0$.

Before moving on, we summarize. To build a bumpy black hole spacetime, we first select a function ψ_1 which satisfies the Laplace equation (2.2). We find the function γ_1 which satisfies Eqs. (2.3) and (2.4), and then apply the Newman-Janis algorithm to "rotate" the spacetime to nonzero a. The result is given by Eqs. (2.36)–(2.43).

III. MOTION IN BLACK HOLE AND BUMPY BLACK HOLE SPACETIMES

We now discuss motion in these spacetimes. Our focus will be computing the frequencies associated with oscillations in the radial coordinate r, the polar angle θ, and rotations in ϕ about the symmetry axis. These frequencies are typically the direct observables of black hole orbits; it is from measuring these frequencies (or the evolution of these frequencies if the orbit evolves) that one can hope to constrain the properties of black hole candidates.

A. Geodesics of Kerr black holes

As background to our discussion of black hole orbital frequencies, we first briefly review the equations governing black hole geodesic orbits, and some useful reparametrizations for practical computations. One goal of this discussion is to introduce certain quantities which we will use in the remainder of this paper.

As first recognized by Carter [37], geodesic motion for a test mass m in a black hole spacetime is separable with respect to Boyer-Lindquist coordinates t, r, θ, and ϕ. The test body's motion is then completely described by four first-order ordinary differential equations:

$$m^2\Sigma^2\left(\frac{dr}{d\tau}\right)^2 = [(r^2+a^2)E - aL_z]^2 - \Delta[m^2r^2 + (L_z - aE)^2 + Q] \equiv R(r), \tag{3.1}$$

$$m^2\Sigma^2\left(\frac{d\theta}{d\tau}\right)^2 = Q - \cot^2\theta L_z^2 - a^2\cos^2\theta(m^2 - E^2) \equiv \Theta(\theta), \tag{3.2}$$

$$m\Sigma\left(\frac{d\phi}{d\tau}\right) = \csc^2\theta L_z + aE\left(\frac{r^2+a^2}{\Delta} - 1\right) - \frac{a^2L_z}{\Delta} \equiv \Phi(r,\theta), \tag{3.3}$$

$$m\Sigma\left(\frac{dt}{d\tau}\right) = E\left[\frac{(r^2+a^2)^2}{\Delta} - a^2\sin^2\theta\right] + aL_z\left(1 - \frac{r^2+a^2}{\Delta}\right) \equiv T(r,\theta). \tag{3.4}$$

As in the previous section, $\Delta = r^2 - 2Mr + a^2$ and $\Sigma = r^2 + a^2\cos^2\theta$; τ is proper time along the test body's worldline. In developing these equations, one isolates four constants of the motion. One is simply the rest mass itself, $m^2 = -p^\mu p_\mu$; this motivates the definition of the Hamiltonian for test body motion,

$$\mathcal{H} \equiv \tfrac{1}{2}g^{\alpha\beta}p_\alpha p_\beta, \tag{3.5}$$

where the 4-momentum components $p_\mu = mg_{\mu\nu}(dx^\nu/d\tau)$. The other constants are the energy E, axial angular momentum L_z, and "Carter constant" Q, given by

$$E \equiv -p_t, \tag{3.6}$$

$$L_z \equiv p_\phi, \tag{3.7}$$

$$Q \equiv p_\theta^2 + \cos^2\theta[a^2(m^2 - E^2) + \csc^2\theta L_z^2]. \tag{3.8}$$

Given a choice of the constants (E, L_z, Q) and a set of initial conditions, Eqs. (3.1), (3.2), (3.3), and (3.4) completely describe the geodesic motion of a test body near a Kerr black hole. The equations for r and θ can present some problems, however, since their motion includes turning points where $dr/d\tau$ and $d\theta/d\tau$ pass through zero and switch sign. To account for this behavior, it is convenient to reparametrize these motions using angles ψ_r (for the radial motion) and χ (for the polar motion) which smoothly vary from 0 to 2π as the motion oscillates between its extremes.

Consider first the radial motion. We define

$$r = \frac{pM}{1 + e\cos\psi_r}. \tag{3.9}$$

The constants p and e are the orbit's semilatus rectum and eccentricity, respectively. Substituting into Eq. (3.1), it is simple to develop an equation governing ψ_r. Periapsis and apoapsis are given by $r_p = pM/(1+e)$ and $r_a = pM/(1-e)$, respectively. This allows us to relate the constants p and e to the constants E, L_z, and Q: They are the outermost radii for which the radial "potential" goes to zero,

$$R(r_p) = R(r_a) = 0. \tag{3.10}$$

For the polar motion, we note that Eq. (3.2) can be written

$$\Sigma^2\left(\frac{d\theta}{d\tau}\right)^2 = \frac{z^2[a^2(m^2 - E^2)] - z[Q + L_z^2 + a^2(m^2 - E^2)] + Q}{1 - z}, \tag{3.11}$$

where we have introduced $z \equiv \cos^2\theta$. Denote by $z_\pm$ the two roots of the quadratic on the right-hand side of Eq. (3.11). Turning points of the θ motion correspond to $z = z_-$, the smaller of these roots. (The root z_+ is greater than 1, and does not correspond to a turning point.) Transforming back to the angle θ, we find that the minimum polar angle reached by the orbit is

$$\cos\theta_{\min} = \sqrt{z_-}. \tag{3.12}$$

(The maximum angle is $\theta_{\max} = \pi - \theta_{\min}$.) A useful reparametrization of the θ coordinate is

$$\cos\theta = \cos\theta_{\min}\cos\chi, \tag{3.13}$$

where χ accumulates like the angle ψ_r. By substitution in Eq. (3.2), we can easily develop an equation governing the evolution of χ.

Before moving on, we note that Eqs. (3.10) and (3.12) allow us to map from the parameters (E, L_z, Q) to $(p, e, \theta_{\min})$. [Schmidt [32] in fact gives an analytic solution for (E, L_z, Q) as functions of $(p, e, \theta_{\min})$.] Up to initial conditions, either parametrization thus completely specifies an orbit. We will flip between these parametrizations as convenient.

B. Orbital frequencies for black holes

To frame our discussion, we begin by examining the frequencies of motion for normal black hole spacetimes. Our discussion here closely follows that given by Schmidt [32], which uses Hamilton-Jacobi methods to compute black hole orbital frequencies. A useful starting point is to note that in separating the coordinate-space motion, one identifies not only constants of the motion, but also the

action variables

$$J_r \equiv \frac{1}{2\pi}\oint p_r dr = \frac{1}{\pi}\int_{r_p}^{r_a}\frac{\sqrt{R(r)}}{\Delta}dr, \tag{3.14}$$

$$J_\theta \equiv \frac{1}{2\pi}\oint p_\theta d\theta = \frac{2}{\pi}\int_{\theta_{\min}}^{\pi/2}\sqrt{\Theta(\theta)}d\theta, \tag{3.15}$$

$$J_\phi \equiv \frac{1}{2\pi}\oint p_\phi d\phi = L_z. \tag{3.16}$$

It is also useful to define

$$J_t \equiv -E. \tag{3.17}$$

This is a slight abuse of the notation since geodesic motion is not cyclic in t (and hence we cannot define J_t as a closed integral over time), but is convenient for reasons we will illustrate shortly.

At least formally, we can now reparametrize our Hamiltonian (3.5) in terms of the action variables J_μ. Let us write the Hamiltonian so reparametrized as $\mathcal{H}^{(\mathrm{aa})}$. By Hamilton-Jacobi theory, the orbital frequencies are the derivatives of $\mathcal{H}^{(\mathrm{aa})}$ with respect to the action variables:

$$m\omega^i = \frac{\partial \mathcal{H}^{(\mathrm{aa})}}{\partial J_i}. \tag{3.18}$$

For black hole orbits, we cannot explicitly reparametrize the Hamiltonian in this way, making it difficult to calculate the orbital frequencies. However, by using the chain rule, we can reexpress (3.18) in terms of derivatives that are not so difficult to explicitly write out. Following Ref. [32] (modifying its notation slightly), we put

$$P_\beta \doteq (\mathcal{H}, E, L_z, Q). \tag{3.19}$$

Define the matrices $\mathcal{A}$ and $\mathcal{B}$, whose components are

$$\mathcal{A}_\alpha{}^\beta = \frac{\partial P_\alpha}{\partial J_\beta}, \qquad \mathcal{B}_\alpha{}^\beta = \frac{\partial J_\alpha}{\partial P_\beta}. \tag{3.20}$$

By the chain rule, these matrices have an inverse relationship:

$$\mathcal{A}_\alpha{}^\beta \mathcal{B}_\beta{}^\gamma = \delta_\alpha{}^\gamma. \tag{3.21}$$

The components of the matrix $\mathcal{A}$ are directly related to the frequencies we wish to compute. In particular, since P_t is just the invariant Hamiltonian, $m\omega^i = \partial P_t/\partial J_i \equiv \mathcal{A}_t{}^i$. However, the components of the matrix $\mathcal{B}$ are written in a way that is fairly easy to work out. We exploit this to write $m\omega^i = (\mathcal{B}^{-1})_t{}^i$, from which we find

$$m\omega^r = \frac{\partial J_\theta/\partial Q}{(\partial J_r/\partial \mathcal{H})(\partial J_\theta/\partial Q) - (\partial J_r/\partial Q)(\partial J_\theta/\partial \mathcal{H})}, \tag{3.22}$$

$$m\omega^\theta = \frac{-\partial J_r/\partial Q}{(\partial J_r/\partial \mathcal{H})(\partial J_\theta/\partial Q) - (\partial J_r/\partial Q)(\partial J_\theta/\partial \mathcal{H})}, \tag{3.23}$$

$$m\omega^\phi = \frac{(\partial J_r/\partial Q)(\partial J_\theta/\partial L_z) - (\partial J_r/\partial L_z)(\partial J_\theta/\partial Q)}{(\partial J_r/\partial \mathcal{H})(\partial J_\theta/\partial Q) - (\partial J_r/\partial Q)(\partial J_\theta/\partial \mathcal{H})}. \tag{3.24}$$

The partial derivatives of J_r and J_θ appearing here are given by

$$\frac{\partial J_r}{\partial \mathcal{H}} = \frac{1}{2\pi}\oint \frac{r^2}{\sqrt{R(r)}}dr, \tag{3.25}$$

$$\frac{\partial J_r}{\partial Q} = -\frac{1}{4\pi}\oint \frac{1}{\sqrt{R(r)}}dr, \tag{3.26}$$

$$\frac{\partial J_r}{\partial L_z} = -\frac{1}{2\pi}\oint \frac{r(rL_z - 2M(L_z - aE))}{\Delta\sqrt{R(r)}}dr, \tag{3.27}$$

$$\frac{\partial J_r}{\partial E} = \frac{1}{2\pi}\oint \frac{r[rE(r^2 + a^2) - 2Ma(L_z - aE)]}{\Delta\sqrt{R(r)}}dr, \tag{3.28}$$

$$\frac{\partial J_\theta}{\partial \mathcal{H}} = \frac{1}{2\pi}\oint \frac{a^2\cos^2\theta}{\sqrt{\Theta(\theta)}}d\theta, \tag{3.29}$$

$$\frac{\partial J_\theta}{\partial Q} = \frac{1}{4\pi}\oint \frac{1}{\sqrt{\Theta(\theta)}}d\theta, \tag{3.30}$$

$$\frac{\partial J_\theta}{\partial L_z} = -\frac{1}{2\pi}\oint \frac{L_z\cot^2\theta}{\sqrt{\Theta(\theta)}}d\theta, \tag{3.31}$$

$$\frac{\partial J_\theta}{\partial E} = \frac{1}{2\pi}\oint \frac{a^2 E\cos^2\theta}{\sqrt{\Theta(\theta)}}d\theta. \tag{3.32}$$

(The derivatives $\partial J_{r,\theta}/\partial E$ will be needed for a quantity we introduce below.) Schmidt [32] combines these results to give closed-form expressions for the three frequencies $\omega^{r,\theta,\phi}$; we will not repeat these expressions here.

The frequencies $\omega^{r,\theta,\phi}$ are conjugate to the orbit's proper time; they would be measured by an observer who rides on the orbit itself. For our purposes, it will be more useful to convert to frequencies conjugate to the Boyer-Lindquist coordinate time, describing measurements made by a distant observer. The quantity[3]

$$\Gamma \equiv \frac{1}{m}\frac{\partial \mathcal{H}^{(\mathrm{aa})}}{\partial J_t} = -\frac{1}{m}\frac{\partial \mathcal{H}^{(\mathrm{aa})}}{\partial E} \tag{3.33}$$

[3]We have adjusted notation from Schmidt slightly to avoid confusion with our metric function γ.

performs this conversion; the frequencies $\Omega^{r,\theta,\phi} = \omega^{r,\theta,\phi}/\Gamma$ are of observational relevance. Going back to Eqs. (3.20) and (3.21), we find $m\Gamma = (\mathcal{B}^{-1})_t{}^t$, or

$$m\Gamma = \frac{(\partial J_r/\partial E)(\partial J_\theta/\partial Q) - (\partial J_r/\partial Q)(\partial J_\theta/\partial E)}{(\partial J_r/\partial \mathcal{H})(\partial J_\theta/\partial Q) - (\partial J_r/\partial Q)(\partial J_\theta/\partial \mathcal{H})}. \tag{3.34}$$

In the discussion that follows, it will be useful to have weak-field ($p \gg M$) forms of these frequencies as a point of comparison. We begin by we taking the exact expressions for E, L_z, and Q given by Schmidt (Appendix B of Ref. [32]), expand to leading order in a, and then expand in $1/p$. The result is

$$E = m\left[1 - \frac{1-e^2}{2p} + \frac{(1-e^2)^2}{p^2}\left(\frac{3}{8} - \frac{a}{M}\frac{\sin\theta_{\min}}{\sqrt{p}}\right)\right], \tag{3.35}$$

$$L_z^2 + Q = m^2M^2p\left[1 + \frac{3+e^2}{p} + \frac{(3+e^2)^2}{p^2} - \frac{a}{M} \times \left(\frac{2(3+e^2)}{p^{3/2}} + \frac{4(2+e^2)(3+e^2)}{p^{5/2}}\right)\sin\theta_{\min}\right], \tag{3.36}$$

$$\frac{L_z}{\sqrt{L_z^2 + Q}} = \sin\theta_{\min}. \tag{3.37}$$

The orbital frequencies become

$$\Omega^r = \omega^K\left[1 - \frac{3(1-e^2)}{p} + \frac{a}{M}\frac{3(1-e^2)\sin\theta_{\min}}{p^{3/2}}\right], \tag{3.38}$$

$$\Omega^\theta = \omega^K\left[1 + \frac{3e^2}{p} - \frac{a}{M}\frac{3(1+e^2)\sin\theta_{\min}}{p^{3/2}}\right], \tag{3.39}$$

$$\Omega^\phi = \omega^K\left[1 + \frac{3e^2}{p} - \frac{a}{M}\frac{3(1+e^2)\sin\theta_{\min}}{p^{3/2}} + \frac{a}{M}\frac{2}{p^{3/2}}\right], \tag{3.40}$$

where

$$\omega^K = \frac{1}{M}\left(\frac{1-e^2}{p}\right)^{3/2} \tag{3.41}$$

is the Kepler frequency.

C. Orbital frequencies of bumpy black holes

Now examine how the orbital frequencies change if the black hole is bumpy. Begin with the Hamiltonian $\mathcal{H}$. It remains conserved with value $-m^2/2$, but its functional form is shifted:

$$\mathcal{H} = \frac{1}{2}g^{\alpha\beta}p_\alpha p_\beta = -\frac{m^2}{2} = \hat{\mathcal{H}} + \mathcal{H}_1, \tag{3.42}$$

where $\hat{\mathcal{H}}$ is the original (nonbumpy) Hamiltonian and $\mathcal{H}_1$ gathers together the influence of the spacetime's bumpiness. To first order in $b_{\alpha\beta}$,

$$g^{\alpha\beta} = \hat{g}^{\alpha\beta} - b^{\alpha\beta}, \tag{3.43}$$

where

$$b^{\alpha\beta} = \hat{g}^{\alpha\mu}\hat{g}^{\beta\nu}b_{\mu\nu}. \tag{3.44}$$

Combining these expressions, we have

$$\mathcal{H}_1 = -\tfrac{1}{2}\hat{g}^{\alpha\mu}\hat{g}^{\beta\nu}b_{\mu\nu}p_\alpha p_\beta, \tag{3.45}$$

which can be rewritten

$$\mathcal{H}_1 = -\frac{1}{2}b_{\mu\nu}p^\mu p^\nu = -\frac{m^2}{2}b_{\mu\nu}\frac{dx^\mu}{d\tau}\frac{dx^\nu}{d\tau}. \tag{3.46}$$

When we add bumps to a spacetime, shifting the Hamiltonian by $\mathcal{H}_1$, the motion is no longer separable (except for the special case of equatorial motion) and the techniques used in Sec. III B for computing orbital frequencies do not work. However, since the spacetime is "close to" the exact black hole spacetime in a well-defined sense, the motion is likewise "close to" the integrable motion. We can thus take advantage of canonical perturbation theory as described in, for example, Goldstein, Poole, and Safko [38], to calculate how the spacetime's bumps change the frequencies.

The key result which we use is that the shift can be found by suitably averaging $\mathcal{H}_1$:

$$m\delta\omega^i = \frac{\partial\langle\mathcal{H}_1\rangle}{\partial\hat{J}_i}, \qquad m\delta\Gamma = \frac{\partial\langle\mathcal{H}_1\rangle}{\partial\hat{J}_t}. \tag{3.47}$$

Notice that the derivatives are taken with respect to the action variables defined for the background motion; the averaging, which we denote with angular brackets, is likewise done with respect to orbits in the background. Once these derivatives are taken, it is simple to compute the changes to the observable frequencies. Expanding

$$\Omega^i = \frac{\omega^i}{\Gamma} = \frac{\hat{\omega}^i + \delta\omega^i}{\hat{\Gamma} + \delta\Gamma} \equiv \hat{\Omega}^i + \delta\Omega^i, \tag{3.48}$$

we read out

$$\delta\Omega^i = \frac{\delta\omega^i}{\hat{\Gamma}} - \frac{\hat{\omega}^i\delta\Gamma}{\hat{\Gamma}^2}, \tag{3.49}$$

or

$$\frac{\delta\Omega^i}{\hat{\Omega}^i} = \frac{\delta\omega^i}{\hat{\omega}^i} - \frac{\delta\Gamma}{\hat{\Gamma}}. \tag{3.50}$$

The averaging used in Eq. (3.47) is described in detail in Appendix A. This procedure uses the fact that the radial and polar components of the background motion can be

separated, and thus can be averaged independently. Following Appendix A, this amounts to computing

$$\langle \mathcal{H}_1 \rangle = \frac{1}{\Upsilon^t (2\pi)^2} \int_0^{2\pi} dw^r \int_0^{2\pi} dw^\theta \mathcal{H}_1[r(w^r), \theta(w^\theta)] \times T[r(w^r), \theta(w^\theta)], \tag{3.51}$$

where $T(r, \theta)$ is defined by Eq. (3.4), where Υ^t is defined by Eq. (A11), and where $w^{r,\theta}$ are angles associated with the separated r and θ motions (defined and discussed in detail in Appendix A).

Before moving on, we discuss a few issues in practically computing $\langle \mathcal{H}_1 \rangle$ and the frequency shifts. Begin by expanding the Hamiltonian:

$$\begin{aligned}\mathcal{H}_1 &= -\frac{m^2}{2}\left[b_{tt}\left(\frac{dt}{d\tau}\right)^2 + b_{rr}\left(\frac{dr}{d\tau}\right)^2 + b_{\theta\theta}\left(\frac{d\theta}{d\tau}\right)^2 + b_{\phi\phi}\left(\frac{d\phi}{d\tau}\right)^2 + 2b_{tr}\frac{dt}{d\tau}\frac{dr}{d\tau} + 2b_{\phi r}\frac{d\phi}{d\tau}\frac{dr}{d\tau} + 2b_{\phi t}\frac{d\phi}{d\tau}\frac{dt}{d\tau}\right] \\ &= -\frac{m^2}{2}\left[b_{tt}\left(\frac{dt}{d\tau}\right)^2 + b_{rr}\left(\frac{dr}{d\tau}\right)^2 + b_{\theta\theta}\left(\frac{d\theta}{d\tau}\right)^2 + b_{\phi\phi}\left(\frac{d\phi}{d\tau}\right)^2 + 2b_{\phi t}\frac{d\phi}{d\tau}\frac{dt}{d\tau}\right] \\ &= -\frac{1}{2\Sigma^2}[b_{tt}T(r,\theta)^2 + b_{rr}R(r) + b_{\theta\theta}\Theta(\theta) + b_{\phi\phi}\Phi(r,\theta)^2 + 2b_{\phi t}\Phi(r,\theta)T(r,\theta)].\end{aligned} \tag{3.52}$$

In going from the first line to the second, we use the fact that terms linear in $dr/d\tau$ go to zero when we average since the radial motion switches sign after half a cycle. The final line of Eq. (3.52) is in a good form for averaging.

In computing this average, we end up with $\langle \mathcal{H}_1 \rangle$ as a function of p, e, and $\theta_{\min}$. We likewise compute the actions J_μ using these parameters, and then compute the shifts to the frequencies and Γ using the chain rule. To set up this calculation, define an array b_β which contains all the system's physical parameters:

$$b_\beta \doteq (m, p, e, \theta_{\min}). \tag{3.53}$$

Next, define the matrix $\mathcal{J}$, the Jacobian of the actions with respect to these parameters:

$$(\mathcal{J})_\alpha{}^\beta = \frac{\partial J_\alpha}{\partial b_\beta}. \tag{3.54}$$

Then,

$$\delta\omega^i = \frac{\partial \langle \mathcal{H}_1 \rangle}{\partial b_\alpha} (\mathcal{J}^{-1})_\alpha{}^i, \tag{3.55}$$

$$\delta\Gamma = \frac{\partial \langle \mathcal{H}_1 \rangle}{\partial b_\alpha} (\mathcal{J}^{-1})_\alpha{}^t, \tag{3.56}$$

where $\mathcal{J}^{-1}$ is the matrix inverse of the Jacobian $\mathcal{J}$.

IV. RESULTS I: ORBITS OF BUMPY SCHWARZSCHILD BLACK HOLES

We now examine spacetimes and orbits for specific choices of ψ_1. Recalling that this function satisfies the Laplace equation, we take ψ_1 to be a pure multipole in the "Weyl sector" [i.e., in the coordinates of Eq. (2.1)]. As we will show in this section and the next, this smooths out the bumps and cures the strong-field pathologies associated with orbits in the spacetimes developed in CH04.

Note that a pure multipole in the Weyl sector will not correspond to a pure Geroch-Hansen moment of the black hole. For example, taking ψ_1 to be proportional to an $l = 2$ spherical harmonic does not change only the moment M_2 of the Geroch-Hansen sequence [Eq. (1.1)]. However, it turns out that taking ψ_1 to be proportional to a spherical harmonic Y_{l0} changes no Geroch-Hansen moments lower than M_l: taking ψ_1 to be an $l = 2$ harmonic changes M_2 and higher moments; taking it to be an $l = 3$ harmonic changes M_3 and higher; etc. A companion paper [28] demonstrates this explicitly, and further shows that the dominant change for $\psi_1 \propto Y_{l0}$ is to the lth Geroch-Hansen moment. Further, since the equations governing ψ_1 and γ_1 are linear in these fields, one can choose ψ_1 to be a combination of multipoles such that the resulting spacetime puts its "bump" into a single Geroch-Hansen moment. In this way, one can arbitrarily adjust the Geroch-Hansen moments of a spacetime (providing that the adjustments are small).

We begin with spacetimes and orbits of bumpy Schwarzschild black holes.

A. Quadrupole bumps ($l = 2$)

First we examine an $l = 2$ perturbation in the Weyl sector. The perturbation ψ_1 which satisfies Eq. (2.2) and has an $l = 2$ spherical harmonic form is

$$\begin{aligned}\psi_1^{l=2}(\rho, z) &= B_2 M^3 \frac{Y_{20}(\theta_{\rm Weyl})}{(\rho^2 + z^2)^{3/2}} \\ &= \frac{B_2 M^3}{4}\sqrt{\frac{5}{\pi}}\frac{3\cos^2\theta_{\rm Weyl} - 1}{(\rho^2 + z^2)^{3/2}},\end{aligned} \tag{4.1}$$

where $\cos\theta_{\rm Weyl} = z/\sqrt{\rho^2 + z^2}$. The dimensionless constant B_2 sets the magnitude of the spacetime's bumpiness for this multipole. Since we are treating the bumpiness as a perturbation, $B_2 \ll 1$. Transforming to Schwarzschild coordinates by Eqs. (2.7), (2.8), (2.12), and (2.13), we find

$$\psi_1^{l=2}(r, \theta) = \frac{B_2 M^3}{4}\sqrt{\frac{5}{\pi}}\frac{1}{d(r,\theta)^3}\left[\frac{3(r - M)^2\cos^2\theta}{d(r,\theta)^2} - 1\right], \tag{4.2}$$

where

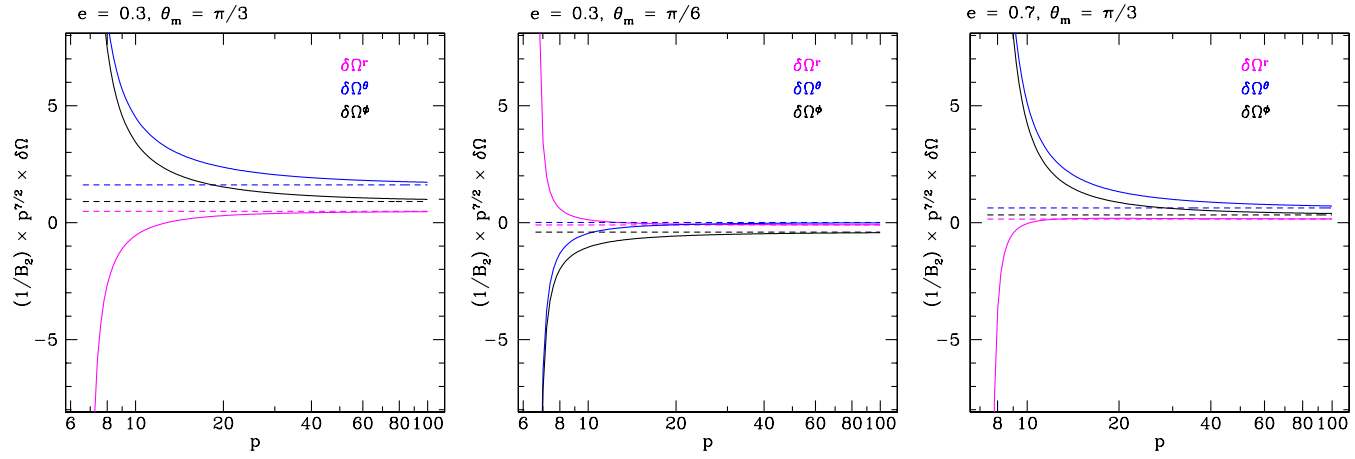

FIG. 1 (color online). Shifts to black hole orbital frequencies due to an $l = 2$ bump. The shifts $\delta\Omega^{r,\theta,\phi}$ are normalized by the bumpiness parameter B_2, and are scaled by $p^{7/2}$; this is because in the Newtonian limit, $\delta\Omega^{r,\theta,\phi} \propto p^{-7/2}$. The Newtonian limit (dashed lines) does a good job of describing the exact calculations (solid lines) for large p. This limit substantially underestimates the shifts in the strong field. Notice that the radial frequency shift changes sign in the strong field, typically at $p \sim (10\text{–}13)M$, depending slightly on parameters. This behavior is starkly different from the weak-field limit.

$$d(r,\theta) \equiv (r^2 - 2Mr + M^2\cos^2\theta)^{1/2}. \tag{4.3}$$

As a useful aside, the mapping from (ρ, z) to (r, θ) implies that any Weyl sector ψ_1 can be transformed into Schwarzschild coordinates by putting

$$\rho^2 + z^2 \to d(r,\theta), \tag{4.4}$$

$$\cos\theta_{\rm Weyl} \to \frac{(r-M)}{d(r,\theta)}\cos\theta. \tag{4.5}$$

Integrating the constraint (2.11) and imposing the condition $\gamma_1(r \to \infty) = 0$ gives

$$\gamma_1^{l=2}(r,\theta) = B_2\sqrt{\frac{5}{\pi}}\left[\frac{(r-M)}{2}\frac{[c_{20}(r) + c_{22}(r)\cos^2\theta]}{d(r,\theta)^5} - 1\right], \tag{4.6}$$

where

$$c_{20}(r) = 2(r-M)^4 - 5M^2(r-M)^2 + 3M^4, \tag{4.7}$$

$$c_{22}(r) = 5M^2(r-M)^2 - 3M^4. \tag{4.8}$$

Figure 1 shows the impact of an $l = 2$ bump on orbital frequencies as a function of p for a few choices of e and θ_m. We show the three shifts $\delta\Omega^{r,\theta,\phi}$, normalized by the bumpiness B_2 and rescaled by the asymptotic weak-field dependence $\delta\Omega^x_{l=2} \propto p^{-7/2}$ (derived in Appendix B). As we move to the weak field, the numerical results (solid lines) converge to the weak-field forms (dashed lines). The frequency shifts generically get substantially larger as we move into the strong field. The bumps have a very strong influence near the last stable orbit, $p_{\rm LSO} = (6 + 2e)$, although the behavior is smooth and nonpathological.

B. Octupole bumps ($l = 3$)

Next, consider an $l = 3$ perturbation. In Weyl coordinates, we put

$$\psi_1^{l=3}(\rho, z) = B_3M^4\frac{Y_{30}(\theta_{\rm Weyl})}{(\rho^2 + z^2)^2}. \tag{4.9}$$

In Schwarzschild coordinates, this becomes

$$\psi_1^{l=3}(r,\theta) = \frac{B_3M^4}{4}\frac{1}{d(r,\theta)^4}\sqrt{\frac{7}{\pi}}\left[\frac{5(r-M)^3\cos^3\theta}{d(r,\theta)^3} - \frac{3(r-M)\cos\theta}{d(r,\theta)}\right]. \tag{4.10}$$

From the constraint equation (2.11) and the condition $\gamma_1(r \to \infty) = 0$, we find

$$\gamma_1^{l=3}(r,\theta) = \frac{B_3M^5}{2}\sqrt{\frac{7}{\pi}}\cos\theta\left[\frac{c_{30}(r) + c_{32}(r)\cos^2\theta + c_{34}(r)\cos^4\theta + c_{36}(r)\cos^6\theta}{d(r,\theta)^7}\right], \tag{4.11}$$

where

$$c_{30}(r) = -3r(r-2M), \tag{4.12}$$

$$c_{32}(r) = 10r(r-2M) + 2M^2, \tag{4.13}$$

$$c_{34}(r) = -7r(r-2M), \tag{4.14}$$

$$c_{36}(r) = -2M^2. \tag{4.15}$$

Notice that $\psi_1^{l=3}$ and $\gamma_1^{l=3}$ are proportional to $\cos\theta$. As such, their contribution to the averaged Hamiltonian $\langle \mathcal{H}_1 \rangle$ is zero: There is no secular shift to orbital frequencies from $l = 3$ bumps. This is identical to the result in Newtonian gravity, as discussed in Appendix B, and holds for all odd values of l.

As in the Newtonian limit, there will be nonsecular shifts to the motion which cannot be described by our orbit-averaged approach. These shifts would be apparent in a direct (time-domain) evolution of the geodesics of spacetimes with odd l bumps. It would be a useful exercise to examine these effects and ascertain under which conditions odd l spacetime bumps could, in principle, have an observable impact.

C. Hexadecapole bumps ($l = 4$)

We conclude our discussion of Schwarzschild bumps with $l = 4$:

$$\psi_1^{l=4}(\rho, z) = B_4 M^5 \frac{Y_{40}(\theta_{\rm Weyl})}{(\rho^2 + z^2)^{5/2}}, \tag{4.16}$$

from which we obtain

$$\psi_1^{l=4}(r,\theta) = \frac{B_4 M^5}{16} \frac{1}{d(r,\theta)^5} \sqrt{\frac{9}{\pi}} \left[\frac{35(r-M)^4 \cos^4\theta}{d(r,\theta)^4} - \frac{30(r-M)^2\cos^2\theta}{d(r,\theta)^2} + 3 \right]. \tag{4.17}$$

Solving for γ_1 as before, we find

$$\gamma_1^{l=4}(r,\theta) = B_4 \sqrt{\frac{9}{\pi}} \left[\frac{(r-M)}{2} \times \frac{c_{40}(r) + c_{42}(r)\cos^2\theta + c_{44}(r)\cos^4\theta}{d(r,\theta)^9} - 1 \right], \tag{4.18}$$

where

$$c_{40}(r) = 8(r-M)^8 - 36M^2(r-M)^6 + 63M^4(r-M)^4 - 50M^6(r-M)^2 + 15M^8, \tag{4.19}$$

$$c_{42}(r) = 36M^2(r-M)^6 - 126M^4(r-M)^4 + 120M^6(r-M)^2 - 30M^8, \tag{4.20}$$

$$c_{44}(r) = 63M^4(r-M)^4 - 70M^6(r-M)^2 + 15M^8. \tag{4.21}$$

Figure 2 presents the same orbits as are shown in Fig. 1 for $l = 4$. The shifts are normalized by the bumpiness B_4 and rescaled by the weak-field form $\delta\Omega^x_{l=4} \propto p^{-11/2}$. The qualitative behavior is largely the same as for the quadrupole bump. In particular, we see once again that there are no strong-field pathologies in the orbit shifts, and that the degree of shift due to spacetime bumps is especially strong near the last stable orbit. The strong-field radial oscillations in $\delta\Omega^r$ are even more pronounced than they were in the

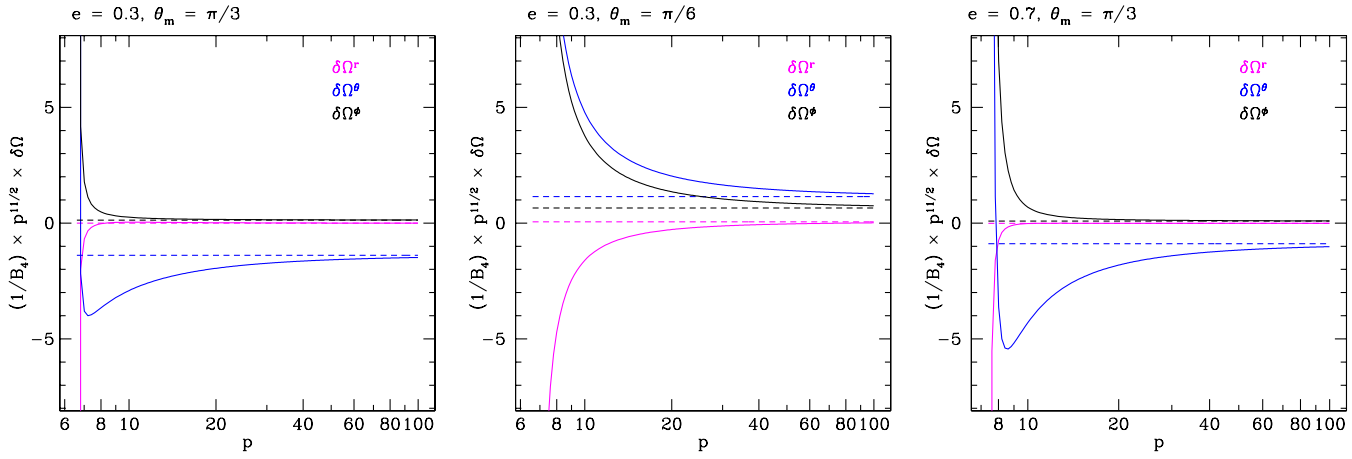

FIG. 2 (color online). Shifts to black hole orbital frequencies due to an $l = 4$ bump. The shifts $\delta\Omega^{r,\theta,\phi}$ are normalized by the bumpiness parameter B_4, and are scaled by $p^{11/2}$, which sets the scaling in the Newtonian limit. As in the $l = 2$ case (Fig. 1), exact results and the Newtonian limit coincide at large p, but there are significant differences in the strong field. The functional behavior of the radial frequency shift can be especially complicated in this case.

$l = 2$ case. This appears to be a robust signature of non-Kerr multipoles in the strong field.

V. RESULTS II: ORBITS OF BUMPY KERR BLACK HOLES

We now repeat the above exercises on a Kerr black hole background.

A. Quadrupole bumps ($l = 2$)

We begin with an $l = 2$ perturbation in the Weyl sector, starting with Eq. (4.1). Transforming to prolate spheroidal coordinates by Eqs. (2.7) and (2.8), this becomes

$$\psi_1^{l=2}(u, v) = \frac{B_2}{4}\sqrt{\frac{5}{\pi}}\left(\frac{3\cosh^2 u\cos^2 v}{\sinh^2 u\sin^2 v + \cosh^2 u\cos^2 v} - 1\right) \times (\sinh^2 u\sin^2 v + \cosh^2 u\cos^2 v)^{-3/2}. \quad (5.1)$$

The corresponding γ_1 is

$$\gamma_1^{l=2}(u, v) = B_2\sqrt{\frac{5}{\pi}}\left[\frac{\cosh u[4 - \cos 2v + (5\cos 2v - 1)\cosh 2u + \cosh 4u]}{8(\sinh^2 u\sin^2 v + \cosh^2 u\cos^2 v)^{5/2}} - 1\right]. \quad (5.2)$$

Following the logic of the Newman-Janis algorithm, we allow u to be complex, and replace $\cosh^2 u$ with $\cosh u\cosh\bar{u}$ and $\sinh^2 u$ with $(\cosh u\cosh\bar{u} - 1)$. Making the coordinate transformation

$$\cosh u = \frac{r - ia\cos\theta}{M} - 1, \qquad v = \theta \quad (5.3)$$

puts the result in Boyer-Lindquist coordinates:

$$\psi_1^{l=2}(r, \theta) = \frac{B_2 M^3}{4}\sqrt{\frac{5}{\pi}}\frac{1}{d(r, \theta, a)^3}\left[\frac{3L(r, \theta, a)^2\cos^2\theta}{d(r, \theta, a)^2} - 1\right], \quad (5.4)$$

$$\gamma_1^{l=2}(r, \theta) = B_2\sqrt{\frac{5}{\pi}}\left[\frac{L(r, \theta, a)}{2}\frac{[c_{20}(r, a) + c_{22}(r, a)\cos^2\theta + c_{24}(r, a)\cos^4\theta]}{d(r, \theta, a)^5} - 1\right], \quad (5.5)$$

where

$$d(r, \theta, a) = \sqrt{r^2 - 2Mr + (M^2 + a^2)\cos^2\theta}, \quad (5.6)$$

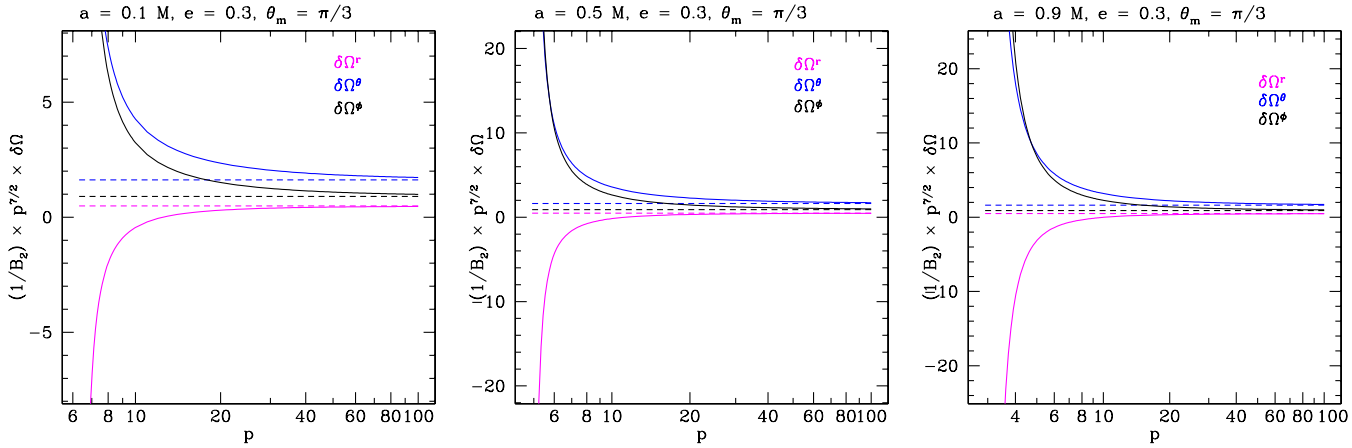

FIG. 3 (color online). Shifts to Kerr black hole orbital frequencies for an $l = 2$ bump. As with the Schwarzschild results presented in Fig. 1, the shifts $\delta\Omega^{r,\theta,\phi}$ are normalized by the bumpiness B_2 and scaled by $p^{7/2}$. Rather than examining a variety of orbital geometries, we here examine a few black hole spins, showing results for $a = 0.1M$, $a = 0.5M$, and $a = 0.9M$. Qualitatively, the results are very similar to what we find for the Schwarzschild case. The major difference is that the last stable orbit is located at smaller p, so that these orbits can get deeper into the strong field. The overall impact of the bumps is greater in these cases which reach deeper into the strong field.

$$L(r,\theta,a) = \sqrt{(r-M)^2 + a^2\cos^2\theta}, \tag{5.7}$$

and

$$c_{20}(r,a) = 2(r-M)^4 - 5M^2(r-M)^2 + 3M^4, \tag{5.8}$$

$$c_{22}(r,a) = 5M^2(r-M)^2 - 3M^4 + a^2[4(r-M)^2 - 5M^2], \tag{5.9}$$

$$c_{24}(r,a) = a^2(2a^2 + 5M^2). \tag{5.10}$$

Note that the result for ψ_1 can be found by taking the Weyl-sector perturbation given by Eq. (4.1) and putting

$$\rho^2 + z^2 \to d(r,\theta,a), \tag{5.11}$$

$$\cos\theta_{\rm Weyl} \to \frac{L(r,\theta,a)}{d(r,\theta,a)}\cos\theta. \tag{5.12}$$

This is the Kerr analog to the mapping described in Eqs. (4.4) and (4.5).

Figure 3 shows how an $l = 2$ bump changes Kerr orbital frequencies. We focus here on how black hole spin affects our results, presenting results for a single orbit geometry ($e = 0.3$, $\theta_m = \pi/3$). The major impact of black hole spin is to change the value of p at which orbits become unstable. For large spin, orbits can reach deeper into the strong field, accumulating larger anomalous shifts to their orbital frequencies. Aside from this behavior, spin has relatively little effect on the shifts: the three panels are similar to one another and to the Schwarzschild result (compare the leftmost panel of Fig. 1). Similar results hold for other orbital geometries, so we confine our plots to these results.

B. Octupole bumps ($l = 3$)

For the $l = 3$ Kerr bump, we begin with Eq. (4.9), then follow the same procedure to take it to Boyer-Linquist coordinates as described for the $l = 2$ Kerr bump. The result is

$$\psi_1^{l=3}(r,\theta) = \frac{B_3 M^4}{4}\sqrt{\frac{7}{\pi}}\frac{1}{d(r,\theta,a)^4}\left[\frac{5L(r,\theta,a)^3\cos^3\theta}{d(r,\theta,a)^3} - \frac{3L(r,\theta,a)\cos\theta}{d(r,\theta,a)}\right], \tag{5.13}$$

$$\gamma_1^{l=3}(r,\theta) = \frac{B_3 M^5}{2}\sqrt{\frac{7}{\pi}}\cos\theta\left[\frac{c_{30}(r,a) + c_{32}(r,a)\cos^2\theta + c_{34}(r,a)\cos^4\theta + c_{36}(r,a)\cos^6\theta}{d(r,\theta,a)^7}\right], \tag{5.14}$$

where

$$c_{30}(r,a) = -3r(r-2M), \tag{5.15}$$

$$c_{32}(r,a) = 10r(r-2M) + 2M^5 - 3a^2, \tag{5.16}$$

$$c_{34}(r,a) = -7r(r-2M) + 10a^2, \tag{5.17}$$

$$c_{36}(r,a) = -2M^2 - 7a^2. \tag{5.18}$$

As with the Schwarzschild $l = 3$ bumps, $\psi_1^{l=3}$ and $\gamma_1^{l=3}$ are proportional to $\cos\theta$, so that $\langle \mathcal{H}_1 \rangle = 0$. Thus, for Kerr as for Schwarzschild, there is no secular shift to orbital frequencies for $l = 3$, or any other odd value of l. We emphasize again that there will be nonsecular shifts to the motion which our orbit-averaged approach misses by construction, and that it would be worthwhile to investigate their importance in future work.

C. Hexadecapole bumps ($l = 4$)

For $l = 4$, we begin with Eq. (4.16). Repeating our procedure to take this into a Kerr bump, we find

$$\psi_1^{l=4}(r,\theta) = \frac{B_4 M^5}{16}\sqrt{\frac{9}{\pi}}\frac{1}{d(r,\theta,a)^5}\left[\frac{35L(r,\theta,a)^4\cos^4\theta}{d(r,\theta,a)^4} - \frac{30L(r,\theta,a)^2\cos^2\theta}{d(r,\theta,a)^2} + 3\right], \tag{5.19}$$

$$\gamma_1^{l=4}(r,\theta) = B_4\sqrt{\frac{9}{\pi}}\left[\frac{L(r,\theta,a)}{8}\frac{[c_{40}(r,a) + c_{42}(r,a)\cos^2\theta + c_{44}(r,a)\cos^4\theta + c_{46}(r,a)\cos^6\theta + c_{48}(r,a)\cos^8\theta]}{d(r,\theta,a)^9} - 1\right], \tag{5.20}$$

where

$$c_{40}(r,a) = 8(r-M)^8 - 36M^2(r-M)^6 + 63M^4(r-M)^4 - 50M^6(r-M)^2 + 15M^8, \quad (5.21)$$

$$c_{42}(r,a) = 36M^2(r-M)^6 - 126M^4(r-M)^4 + 120M^6(r-M)^2 - 30M^8 + 2a^2[16(r-M)^6 - 54M^2(r-M)^4 + 63M^4(r-M)^2 - 25M^6], \quad (5.22)$$

$$c_{44}(r,a) = 63M^4(r-M)^4 - 70M^6(r-M)^2 + 15M^8 + 3a^2[4M^2(9(r-M)^4 - 21M^2(r-M)^2 + 10M^4) + a^2(16(r-M)^4 - 36M^2(r-M)^2 + 21M^4)], \quad (5.23)$$

$$c_{46}(r,a) = 2a^2[2a^4(8(r-M)^2 - 9M^2) + 9a^2M^2(6(r-M)^2 - 7M^2) + 7M^4(9(r-M)^2 - 5M^2)], \quad (5.24)$$

$$c_{48}(r,a) = a^4(8a^4 + 36a^2M^2 + 63M^4). \quad (5.25)$$

It is a straightforward exercise to numerically compute $\delta\Omega^{r,\theta,\phi}$ using $\psi_1^{l=4}$ and $\gamma_1^{l=4}$ and build the Kerr analogs to the results we show in Fig. 2. The results are not markedly different from those for Schwarzschild, modulo the fact that the orbit can (especially for large spin) reach deeper into the strong field and hence accumulate more bump-induced anomalous precession. Since there are no particularly surprising features in these results compared to what we have already shown, we will not show such plots.

VI. SUMMARY AND FUTURE WORK

This analysis significantly improves on the earlier presentation of bumpy black holes given in CH04, producing bumps with well-behaved strong-field structure, and extending the concept to Kerr black holes. These extensions greatly expand the astrophysical relevance of these spacetimes. We have also demonstrated how Hamilton-Jacobi theory can be applied to orbits in bumpy spacetimes to categorize the anomalous precessions arising from their bumps in a reasonably straightforward manner. Bumpy black holes can now, at least in principle, be used as the foundation for strong-gravity tests with astrophysical data.

It is worth reemphasizing why we propose to use bumpy black holes, rather than using exact solutions which include black holes as a limit (for example, the Novikov-Manko spacetime [31] used in Ref. [30]). In large part, our choice is a matter of taste. Our goal is to tweak a black hole's moments in an arbitrary manner, so that the non-Kerr nature is entirely under our control. From the standpoint of formulating a null experiment, it arguably makes no difference whether the Kerr deviation takes one particular form or another. Any falsifiable non-Kerr form is good enough to formulate the test. To our minds, the nice feature of this approach is that if, for example, a theory of gravity specifies that a black hole should have the same moment structure as general relativity up to some $l = L$, it is simple to design a spacetime tailored to testing that theory. The case of Chern-Simons gravity discussed in Ref. [25] shows that this motivation is not merely academic, but is motivated by plausible alternatives to general relativity.

This analysis provides a complete description of "mass-type" bumps, i.e., perturbations to the mass moments M_l. We have not examined "current-type bumps," shifts to the spin moments S_l. It is also worth bearing in mind that a pure multipole in the Weyl sector, $\psi_1^l \propto Y_{l0}(\theta)$ does not correspond to a shift in a pure Geroch-Hansen multipole. A companion paper by one of us (S. J. V.) addresses these issues [28]. That analysis shows how spin moments can be adjusted from their Kerr values by perturbing the Ernst potential describing the spacetime [27]. It also shows that a pure Weyl-sector multipole ψ_1^l changes no Geroch-Hansen moments lower than l. As such, a pure Geroch-Hansen moment perturbation can be assembled by combining multiple Weyl-sector multipole perturbations.

Aside from these more formal issues, the next major step in this program will be to use these foundations to formulate actual strong-field gravity tests that can be applied to astrophysical data. We imagine several directions that would be interesting to follow:

(i) *Extreme mass ratio inspiral (EMRI)*: The capture and inspiral of stellar mass compact into massive black holes at galaxy centers is one of the original motivations of this work. Much of the recent literature on testing and mapping black hole spacetimes has centered on understanding the character of orbits in non-Kerr black hole candidate spacetimes [15,29,39], with an eye on application to gravitational-wave measurement of EMRIs.
The full analysis of EMRIs in non-Kerr spacetimes is, in principle, quite complicated since their non-Kerr-ness breaks the Petrov type D character of Kerr black holes. As such, it may be quite difficult to accurately compute their radiation emission. It may not be quite so difficult in bumpy black hole spacetimes. Thanks to the smallness of their non-Kerr character, it may be fruitful to use a "hybrid" approach in which the short time scale motion is computed in the bumpy spacetime, but the radiation generation and backreaction is computed in the Kerr spacetime; a similar idea was suggested in the context of modeling EMRI events in Chern-Simons gravity [40]. Given that our goal is to formulate a null experiment, this hybrid may be good enough for

a useful test, in lieu of solving the entire radiation reaction problem in non-Kerr spacetimes.

(ii) *Black hole–pulsar systems*: One of the goals of the planned Square Kilometer Array [6] is the discovery of a black hole–pulsar binary system. If such a system is discovered, detailed observation over many years should be able to tease the multipole structure of the black hole from the data. Similar observations of neutron star–pulsar binary systems have already allowed us to make exquisite measurements of neutron star properties and gravitational-wave emission [41]. The tools developed here may already be adequate for doing this analysis since such binaries will have a relatively slow inspiral time.

(iii) *Accretion flows on black hole candidate*: Programs to observe the (presumed) black hole at the center of our galaxy are maturing very quickly; programs to study accretion flows onto stellar mass black holes in x rays are already quite mature. In our galactic center, the most precise measurements come from millimeter wavelength radio emission from gas accreting onto this central object. The precision of these measurements is increasing to the point where we will soon be able to use them to map the detailed strong-field spacetime structure of the spacetime near Sagittarius A*. It would be a worthwhile exercise to repeat analyses of the appearance of these flows in Kerr spacetimes [42] for bumpy spacetimes to see how accurately such measurements may be able to probe the central object's multipoles. Such an analysis will require developing imaging maps of bumpy black holes, going beyond the orbit frequency analysis we have given here. In the domain of x rays, it would be very interesting to extend work on quiescent accretion flows (as in, for example, Ref. [5]) to include accretion in bumpy black hole spacetimes. It may be possible to extend those analyses to fit for multipoles beyond the black hole's mass and spin.

ACKNOWLEDGMENTS

We thank Dimitrios Psaltis for useful feedback on bumpy black holes in the early stage of this project, and for very helpful discussions about testing black hole spacetimes with observations at the galactic center. We also thank Avi Loeb for discussion about galactic center observations, Ilya Mandel for helpful advice and pointers to the literature as we were completing this paper, and Tim Johannsen and Nico Yunes for useful feedback on a preprint of this paper. The package MATHEMATICA was used to facilitate many of our calculations, both analytic and numerical. This work was supported by NSF Grant No. PHY-0449884, and by NASA Grants No. NNG05G105G and No. NNX08AL42G; S. A. H. in addition gratefully acknowledges the support of the Adam J. Burgasser Chair in Astrophysics at MIT in completing this analysis.

APPENDIX A: AVERAGING FUNCTIONS ALONG BLACK HOLE ORBITS

Key to computing the shifts that a black hole's bumps impart to its orbital frequencies is averaging the Hamiltonian perturbation $\mathcal{H}_1 = \mathcal{H}_1(r, \theta)$ along the orbit. The averaging we wish to use is a time average:

$$\langle \mathcal{H}_1 \rangle = \lim_{T\to\infty} \frac{1}{2T} \int_{-T}^{T} \mathcal{H}_1[r(t), \theta(t)]dt. \tag{A1}$$

Implementing this integral is somewhat involved, so we review the procedure here. These details were first developed by Drasco and Hughes (Ref. [34]), hereafter DH04.

Most GR textbooks (e.g., Ref. [8], Chap. 33) describe the motion of a small test body orbiting a Kerr black hole using Eqs. (3.1), (3.2), (3.3), and (3.4). Although the coordinate motions are formally separated in these equations, in a practical application they are not quite "separated enough" thanks to the factors of $\Sigma = r^2 + a^2\cos^2\theta$ which appear on the left-hand side of these equations. These factors couple the radial and polar motion, and complicate averaging functions of the form $f(r, \theta)$ that are computed on an orbit. Unless the r and θ periods coincide (or are in an integer ratio), one cannot easily average over the r and θ motion.

This residual coupling is eliminated by parametrizing the orbits using what is now often called "Mino time" λ, defined by $d\lambda = d\tau/\Sigma$. Equations (3.1), (3.2), (3.3), and (3.4) become

$$\left(\frac{dr}{d\lambda}\right)^2 = R(r), \tag{A2}$$

$$\left(\frac{d\theta}{d\lambda}\right)^2 = \Theta(\theta), \tag{A3}$$

$$\frac{d\phi}{d\lambda} = \Phi(r, \theta), \tag{A4}$$

$$\frac{dt}{d\lambda} = T(r, \theta). \tag{A5}$$

Since this time variable explicitly separates the r and θ motion, it is simple to construct $r(\lambda)$ using Eq. (A2), and likewise to construct $\theta(\lambda)$ with (A3). It is also simple to compute the r and θ periods in Mino time: By inspection of Eqs. (A2) and (A3), and taking into account symmetries of the motion and the appropriate functions, we have

$$\Lambda^r = 2\int_{r_p}^{r_a} \frac{dr}{\sqrt{R(r)}}, \tag{A6}$$

$$\Lambda^\theta = 4\int_{\theta_{\min}}^{\pi/2} \frac{d\theta}{\sqrt{\Theta(\theta)}}. \tag{A7}$$

Following DH04, we define frequencies conjugate to these periods,

$$\Upsilon^{r,\theta} = 2\pi/\Lambda^{r,\theta}, \tag{A8}$$

and then introduce angles

$$w^{r,\theta} = \Upsilon^{r,\theta}\lambda. \tag{A9}$$

We then write the radial motion as a function of w^r,

$$r(w^r) = r(\lambda = w^r/\Upsilon^r); \tag{A10}$$

we likewise parametrize the polar motion using w^θ. The key concept behind the averaging is that we now allow the angles w^r and w^θ to separately vary. This allows us to separately average the r and θ motions.

We are nearly ready to use these tools to average our Hamiltonian. Before doing so, we define Υ^t, the time function $T(r, \theta)$ averaged over the angles w^r and w^θ:

$$\Upsilon^t \equiv \frac{1}{(2\pi)^2}\int_0^{2\pi} dw^r \int_0^{2\pi} dw^\theta T[r(w^r), \theta(w^\theta)]. \tag{A11}$$

[In DH04, this quantity was denoted by a capital gamma; we are adjusting the notation slightly to avoid conflict with Γ as defined in Eq. (3.34). It is something of an abuse of our notation, since the time t is not periodic and Υ^i typically denotes a frequency.]

As shown in DH04, it is now simple to compute the long-time average of any black hole orbit functional:

$$\begin{aligned}\langle f\rangle &\equiv \lim_{T\to\infty}\frac{1}{2T}\int_{-T}^{T} f[r(t), \theta(t)]dt \\ &= \frac{1}{\Upsilon^t(2\pi)^2}\int_0^{2\pi} dw^r \int_0^{2\pi} dw^\theta f[r(w^r), \theta(w^\theta)] \\ &\quad \times T[r(w^r), \theta(w^\theta)].\end{aligned} \tag{A12}$$

This is the procedure we use to compute $\langle \mathcal{H}_1\rangle$ for all the computations presented in this paper.

APPENDIX B: NEWTONIAN PRECESSION FREQUENCIES

For weak-field orbits, we expect that the bumpy black hole frequency shifts [Eqs. (3.47), (3.48), (3.49), and (3.50)] are well described using Newtonian gravity. In this appendix, we compute the relevant Newtonian frequency shifts; in Secs. IV and V, we show that our general formulas limit to the results we develop here for large radius orbits.

As in our relativistic calculation, we compute frequency shifts due to multipolar "bumps" by examining the variation of a perturbed Hamiltonian with respect to an orbit's action variables:

$$m\delta\Omega^i = \frac{\partial\langle\mathcal{H}_1\rangle}{\partial J_i}. \tag{B1}$$

(Since there is no distinction between coordinate and proper time in Newtonian gravity, these $\delta\Omega^i$ are the measurable frequencies.) The actions are defined just as in the relativistic case, Eqs. (3.14), (3.15), and (3.16). For a body of mass m orbiting a mass M in Newtonian gravity, they become

$$J_r = m\sqrt{pM}\left(\sqrt{\frac{1}{1-e^2}} - 1\right), \tag{B2}$$

$$J_\theta = m\sqrt{pM}(1 - \sin\theta_m), \tag{B3}$$

$$J_\phi = m\sqrt{pM}\sin\theta_m. \tag{B4}$$

The perturbation to the Hamiltonian for orbits is proportional to the perturbation to the potential:

$$\mathcal{H}_1^{\text{Newt}} = m\delta V_l(r, \theta) = \frac{mB_l M^{l+1}}{r^{l+1}}Y_{l0}(\cos\theta). \tag{B5}$$

To perform the averaging, we first reparametrize both the radial and angular motion in a manner similar to what we use for black hole orbits:

$$r = \frac{pM}{1 + e\cos\psi_r}, \tag{B6}$$

$$\cos\theta = \cos\theta_m\cos(\psi_r - \chi_0). \tag{B7}$$

Notice that the radial and angular motions vary in phase with one another in the Newtonian limit: both complete a full cycle as the angle ψ_r varies from 0 to 2π. The angle χ_0 is an offset phase between these motions. Inserting this parametrization into the Newtonian equations of orbital motion, we find

$$\frac{d\psi_r}{dt} = \sqrt{\frac{M}{p^3}}(1 + e\cos\psi_r)^2. \tag{B8}$$

The averaged Hamiltonian is then given by

$$\begin{aligned}\langle\mathcal{H}_1^{\text{Newt}}\rangle &= \frac{m}{T_K}\int_0^{T_K}\delta V_l[r(t), \theta(t)]dt \\ &= \frac{m}{T_K}\int_0^{2\pi}\left(\frac{d\psi_r}{dt}\right)^{-1}\delta V_l[r(\psi_r), \cos\theta(\psi_r)]d\psi_r,\end{aligned} \tag{B9}$$

where $T_K = 2\pi M\sqrt{p^3/(1-e^2)^3}$ is the Keplerian orbital period. [To put this in a more familiar form, recall that the orbit's semimajor axis $A = pM/(1-e^2)$.]

Using these results, we now examine the Newtonian limit of $l = 2$, 3, and 4 black hole bumps.

1. Quadrupole ($l = 2$)

The quadrupole bump is given by the potential

$$\delta V^{l=2} = \frac{B_2 M^3}{4r^3}\sqrt{\frac{5}{\pi}}[3\cos^2\theta - 1], \tag{B10}$$

for which we find

$$\langle \mathcal{H}_1 \rangle = \frac{mB_2}{8p^3}\sqrt{\frac{5}{\pi}}(1-e^2)^{3/2}(1-3\sin^2\theta_m). \quad \text{(B11)}$$

Varying this averaged Hamiltonian with respect to $J_{r,\theta,\phi}$, we find

$$\delta\Omega^r = \frac{3B_2}{8M}\frac{1}{p^{7/2}}\sqrt{\frac{5}{\pi}}(1-e^2)^2(3\sin^2\theta_m - 1), \quad \text{(B12)}$$

$$\delta\Omega^\theta = \frac{3B_2}{8M}\frac{1}{p^{7/2}}\sqrt{\frac{5}{\pi}}(1-e^2)^{3/2} \times [\sin^2\theta_m(5+3\sqrt{1-e^2}) - \sqrt{1-e^2} - 1], \quad \text{(B13)}$$

$$\delta\Omega^\phi = \frac{3B_2}{8M}\frac{1}{p^{7/2}}\sqrt{\frac{5}{\pi}}(1-e^2)^{3/2} \times [\sin^2\theta_m(5+3\sqrt{1-e^2}) - 2\sin\theta_m - \sqrt{1-e^2} - 1]. \quad \text{(B14)}$$

These frequencies are written using the Kepler frequency $\omega_K = 2\pi/T_K$.

Equations (B12)–(B14) reproduce well-known results for motion in a spherical potential augmented by a quadrupole perturbation. To facilitate comparison with the literature, it is useful to change our description of the orientation of the orbital plane from θ_m (the minimum angle θ reached over an orbit) to $\iota = \pi/2 - \theta_m$ (the orbit's inclination with respect to the equatorial plane). We then construct the precession frequencies

$$\Omega^{\rm apsis} = \delta\Omega^\theta - \delta\Omega^r = \omega^K \times \frac{3B_2}{8M}\frac{1}{p^2}\sqrt{\frac{5}{\pi}}(5\cos^2\iota - 1), \quad \text{(B15)}$$

$$\Omega^{\rm plane} = \delta\Omega^\phi - \delta\Omega^\theta = -\omega^K \times \frac{3B_2}{4M}\frac{1}{p^2}\sqrt{\frac{5}{\pi}}\cos\iota; \quad \text{(B16)}$$

$\Omega^{\rm apsis}$ describes the frequency of the orbit's apsidal precession within its orbital plane, and $\Omega^{\rm plane}$ the frequency at which the orbital plane precesses around the symmetry axis. These frequencies reproduce expressions that can be found in the literature; cf. Sec. 12.3C of Ref. [38], and Sec. 3.6.2 of Ref. [43].

The apsidal precession (B15) is due to beating between the orbit's radial and polar motions. In many relativity applications, one is interested in the precession of an orbit's periastron, which is due to a beat between the orbit's radial and azimuthal motions. For the quadrupole bump, we find

$$\Omega^{\rm peri} = \delta\Omega^\phi - \delta\Omega^r = \omega_K \times \frac{3B_2}{8M}\frac{1}{p^2}\sqrt{\frac{5}{\pi}}(5\cos^2\iota - 2\cos\iota - 1). \quad \text{(B17)}$$

Taking the equatorial limit ($\iota = 0$), we see that this result agrees with Eq. (A4) of CH04 provided we identify their parameter Q with $B_2M^3\sqrt{5/4\pi}$. Comparison of the potential used in CH04 [their Eq. (A4)] with our form [Eq. (B10)] shows that this identification is exactly correct.

2. Octupole shift ($l = 3$)

The octupole bump is given by the potential

$$\delta V^{l=3} = \frac{B_3M^4}{4r^4}\sqrt{\frac{7}{\pi}}[5\cos^3\theta - 3\cos\theta], \quad \text{(B18)}$$

leading to

$$\langle \mathcal{H}_1 \rangle = \frac{3mB_3e}{16p^4}\sqrt{\frac{7}{\pi}}(1-e^2)^{3/2}\cos\theta_m(5\cos^2\theta_m - 4)\cos\chi_0. \quad \text{(B19)}$$

This is proportional to $\cos\chi_0$, and so depends on the phase offset of the radial and angular motions. Over very long time scales, precessions will average out this dependence. However, on time scales that are not long enough for χ_0 to vary over its full range, there is a residual impact, leading to octupolar shifts to observable frequencies. This can be very important in Newtonian celestial mechanics. For black hole applications, where the r and θ motions do not vary in phase with one another, this averaging will be much stronger, and treating $\langle \mathcal{H}_1 \rangle \simeq 0$ should be much more accurate.

Varying the averaged octupole Hamiltonian shift, we find

$$\delta\Omega^r = \frac{3B_3}{16eM}\frac{1}{p^{9/2}}\sqrt{\frac{7}{\pi}}(1-e^2)^2(1-4e^2) \times (5\cos^2\theta_m - 4)\cos\chi_0, \quad \text{(B20)}$$

$$\delta\Omega^\theta = \frac{3B_3}{16eM}\frac{1}{p^{9/2}}\sqrt{\frac{7}{\pi}}(1-e^2)^{3/2} \times [\cos\theta_m[4(1-\sqrt{1-e^2} + 4e^2(1+\sqrt{1-e^2})) + 15e^2\sin^2\theta_m] - 4e^2\sin\theta_m\tan\theta_m - 5[1-\sqrt{1-e^2} + 4e^2(1+\sqrt{1-e^2})] \times \cos^3\theta_m]\cos\chi_0, \quad \text{(B21)}$$

$$\delta\Omega^{\theta} = \frac{3B_3}{16eM}\frac{1}{p^{9/2}}\sqrt{\frac{7}{\pi}}(1-e^2)^{3/2} \times [\cos\theta_m[4-4\sqrt{1-e^2}+16e^2\sqrt{1-e^2} + e^2[16+15(\sin\theta_m-1)]\sin\theta_m] - 4e^2(\sin\theta_m-1)\tan\theta_m - 5[1-\sqrt{1-e^2}+4e^2(1+\sqrt{1-e^2})] \times \cos^3\theta_m]\cos\chi_0. \quad \text{(B22)}$$

As expected from the form of the averaged Hamiltonian, all precession frequencies are proportional to the cosine of the offset phase χ_0. On average we therefore find no influence from the $l=3$ perturbation, nor from any odd l multipolar bump. The ''instantaneous'' impact of odd l bumps is, however, nonzero.

3. Hexadecapole shift ($l=4$)

Finally, for the hexadecapole bump, we have

$$\delta V^{l=4} = \frac{B_4 M^5}{16r^5}\sqrt{\frac{9}{\pi}}[35\cos^4\theta - 30\cos^2\theta + 3], \quad \text{(B23)}$$

leading to

$$\langle\mathcal{H}_1\rangle = \frac{3mB_4}{256p^5}\sqrt{\frac{9}{\pi}}(1-e^2)^{3/2} \times [8(2+3e^2) - 20\cos^2\theta_m(4+6e^2 + 3e^2\cos 2\chi_0) + 35\cos^4\theta_m(2+3e^2+2e^2\cos 2\chi_0)]. \quad \text{(B24)}$$

We focus on the secular (long-time average) precessions, and average this over χ_0, leaving

$$\langle\mathcal{H}_1\rangle = \frac{3mB_4}{256p^5}\sqrt{\frac{9}{\pi}}(1-e^2)^{3/2}(2+3e^2) \times (8-40\cos^2\theta_m+35\cos^4\theta_m). \quad \text{(B25)}$$

The precession frequencies which arise from this are

$$\delta\Omega^{r} = -\frac{45B_4}{256M}\frac{1}{p^{11/2}}\sqrt{\frac{9}{\pi}}(1-e^2)^2 \times (8-40\cos^2\theta_m+35\cos^4\theta_m), \quad \text{(B26)}$$

$$\delta\Omega^{\theta} = -\frac{15B_4}{256M}\frac{1}{p^{11/2}}\sqrt{\frac{9}{\pi}}(1-e^2)^{3/2} \times [8(8+3e^2(3+\sqrt{1-e^2})) - 4(62+e^2(63+30\sqrt{1-e^2}))\cos^2\theta_m + 7(28+3e^2(9+5\sqrt{1-e^2}))\cos^4\theta_m], \quad \text{(B27)}$$

$$\delta\Omega^{\phi} = \delta\Omega^{\theta} + \frac{15B_4}{256M}\frac{1}{p^{11/2}}\sqrt{\frac{9}{\pi}}(1-e^2)^{3/2}(2+3e^2) \times \sin\theta_m(28-40\cos^2\theta_m). \quad \text{(B28)}$$

[1] B. Bertotti, L. Iess, and P. Tortora, Nature (London) **425**, 374 (2003).
[2] M. Kramer, I. H. Stairs, R. N. Manchester, M. A. McLaughlin, A. G. Lyne, R. D. Ferdman, M. Burgay, D. R. Lorimer, A. Possenti, N. D'Amico, J. M. Sarkissian, G. B. Hobbs, J. E. Reynolds, P. C. C. Freire, and F. Camilo, Science **314**, 97 (2006).
[3] S. Doeleman, J. Weintroub, A. E. E. Rogers, R. Plambeck, R. Freund, R. P. J. Tilanus, P. Friberg, L. M. Ziurys, J. M. Moran, B. Corey, K. H. Young, D. L. Smythe, M. Titus, D. P. Marrone, R. J. Cappallo, D. C. J. Bock, G. C. Bower, R. Chamberlin, G. R. Davis, T. P. Krichbaum, J. Lamb, H. Maness, A. E. Niell, A. Roy, P. Strittmatter, D. Werthimer, A. R. Whitney, and D. Woody, Nature (London) **455**, 78 (2008).
[4] D. Psaltis, Living Rev. Relativity **11**, 9 (2008).
[5] R. Narayan, J. E. McClintock, and R. Shafee, AIP Conf. Proc. **968**, 265 (2008).
[6] R. Smits, M. Kramer, B. Stappers, D. R. Lorimer, J. Cordes, and A. Faulkner, Astron. Astrophys. **493**, 1161 (2009).
[7] P. Amaro-Seoane, J. R. Gair, M. Freitag, M. C. Miller, I. Mandel, C. J. Cuterl, and S. Babak, Classical Quantum Gravity **24**, R113 (2007).
[8] C. W. Misner, K. S. Thorne, and J. A. Wheeler, *Gravitation* (W. H. Freeman and Company, New York, 1973).
[9] C. M. Will, *Theory and Experiment in Gravitational Physics* (Cambridge University Press, Cambridge, 1993), revised edition.
[10] W. Israel, Phys. Rev. **164**, 1776 (1967).
[11] B. Carter, Phys. Rev. Lett. **26**, 331 (1971).
[12] D. C. Robinson, Phys. Rev. Lett. **34**, 905 (1975).
[13] R. H. Price, Phys. Rev. D **5**, 2419 (1972).
[14] R. H. Price, Phys. Rev. D **5**, 2439 (1972).
[15] J. Brink, Phys. Rev. D **78**, 102001 (2008).
[16] R. Geroch, J. Math. Phys. (N.Y.) **11**, 2580 (1970).

[17] R. O. Hansen, J. Math. Phys. (N.Y.) **15**, 46 (1974).
[18] N. A. Collins and S. A. Hughes, Phys. Rev. D **69**, 124022 (2004).
[19] M. Colpi, S. L. Shapiro, and I. Wasserman, Phys. Rev. Lett. **57**, 2485 (1986).
[20] F. D. Ryan, Phys. Rev. D **55**, 6081 (1997).
[21] D. Psaltis (private communication).
[22] K. Glampedakis and S. Babak, Classical Quantum Gravity **23**, 4167 (2006).
[23] J. B. Hartle, Astrophys. J. **150**, 1005 (1967).
[24] J. B. Hartle and K. S. Thorne, Astrophys. J. **153**, 807 (1968).
[25] N. Yunes and F. Pretorius, Phys. Rev. D **79**, 084043 (2009).
[26] E. T. Newman and A. I. Janis, J. Math. Phys. (N.Y.) **6**, 915 (1965).
[27] F. J. Ernst, Phys. Rev. **167**, 1175 (1968).
[28] S. J. Vigeland (unpublished).
[29] J. Brink, Phys. Rev. D **78**, 102002 (2008).
[30] J. R. Gair, C. Li, and I. Mandel, Phys. Rev. D **77**, 024035 (2008).
[31] V. S. Manko and I. D. Novikov, Classical Quantum Gravity **9**, 2477 (1992).
[32] W. Schmidt, Classical Quantum Gravity **19**, 2743 (2002).
[33] T. Hinderer and E. E. Flanagan, Phys. Rev. D **78**, 064028 (2008).
[34] S. Drasco and S. A. Hughes, Phys. Rev. D **69**, 044015 (2004).
[35] H. Weyl, Ann. Phys. (Leipzig) **359**, 117 (1917).
[36] S. P. Drake and P. Szekeres, Gen. Relativ. Gravit. **32**, 445 (2000).
[37] B. Carter, Phys. Rev. **174**, 1559 (1968).
[38] H. Goldstein, C. Poole, and J. Safko, *Classical Mechanics* (Addison Wesley, San Francisco, 2002), Secs. 10.8 and 12.3.
[39] T. A. Apostolatos, G. Lukes-Gerakopoulos, and G. Contopolous, Phys. Rev. Lett. **103**, 111101 (2009).
[40] C. F. Sopuerta and N. Yunes, Phys. Rev. D **80**, 064006 (2009).
[41] I. H. Stairs, Living Rev. Relativity **6**, 5 (2003).
[42] A. E. Broderick and A. Loeb, Mon. Not. R. Astron. Soc. **363**, 353 (2005).
[43] M. Capderou, *Satellites: Orbits and Missions* (Springer, Paris, 2005).